Journal of Neuroinflammation

RESEARCH Open Access

Diverse cell types establish a pathogenic immune environment in peripheral neuropathy

Julie Choi[1], Amy Strickland[1], Hui Qi Loo[2], Wendy Dong[1], Lilianne Barbar[2], A. Joseph Bloom[1,3], Yo Sasaki[1], Sheng Chih Jin[1], Aaron DiAntonio[2,3] and Jeffrey Milbrandt[1,3,4*]

Abstract

Neuroinflammation plays a complex and context-dependent role in many neurodegenerative diseases. We identified a key pathogenic function of macrophages in a mouse model of a rare human congenital neuropathy in which SARM1, the central executioner of axon degeneration, is activated by hypomorphic mutations in the axon survival factor NMNAT2. Macrophage depletion blocked and reversed neuropathic phenotypes in this sarmopathy model, revealing SARM1-dependent neuroimmune mechanisms as key drivers of disease pathogenesis. In this study, we investigated the impact of chronic subacute SARM1 activation on the peripheral nerve milieu using single cell/nucleus RNA-sequencing (sc/snRNA-seq). Our analyses reveal an expansion of immune cells (macrophages and T lymphocytes) and repair Schwann cells, as well as significant transcriptional alterations to a wide range of nerve-resident cell types. Notably, endoneurial fibroblasts show increased expression of chemokines (*Ccl9*, *Cxcl5*) and complement components (*C3*, *C4b*, *C6*) in response to chronic SARM1 activation, indicating enhanced immune cell recruitment and immune response regulation by non-immune nerve-resident cells. Analysis of $CD45^+$ immune cells in sciatic nerves revealed an expansion of an $Il1b^+$ macrophage subpopulation with increased expression of markers associated with phagocytosis and T cell activation/proliferation. We also found a significant increase in T cells in sarmopathic nerves. Remarkably, T cell depletion rescued motor phenotypes in the sarmopathy model. These findings delineate the significant changes chronic SARM1 activation induces in peripheral nerves and highlights the potential of immunomodulatory therapies for SARM1-dependent peripheral neurodegenerative disease.

Keywords SARM1, NMNAT2, Sarmopathy, Nerve-resident cells, Endoneurial fibroblasts, Repair Schwann cells, Neuroinflammation, Cytokines, Complement, Macrophages, T cells

*Correspondence:
Jeffrey Milbrandt
jmilbrandt@wustl.edu
[1]Department of Genetics, Washington University School of Medicine, St. Louis, MO 63110, USA
[2]Department of Developmental Biology, Washington University School of Medicine, St. Louis, MO 63110, USA
[3]Needleman Center for Neurometabolism and Axonal Therapeutics, St. Louis, MO 63110, USA
[4]McDonnell Genome Institute, Washington University School of Medicine, St. Louis, MO 63110, USA

Background

Axon degeneration is a hallmark of numerous neurodegenerative diseases, including peripheral neuropathy [1–4]. The process of axon degeneration is largely governed by the balance between the activities of SARM1 (sterile alpha and toll/interleukin-1 receptor motif containing 1), a pro-degenerative enzyme, and NMNAT2 (nicotinamide mononucleotide adenylyl-transferase 2), a pro-survival enzyme [5, 6]. As a labile protein produced in the soma and transported down the axon, NMNAT2 loss or enzymatic dysfunction leads to a buildup of its substrate NMN and depletion of its product NAD^+ [7, 8]. This leads to conformational change and activation of SARM1 through competitive allosteric binding [7, 9]. SARM1 cleaves NAD^+, a crucial cellular metabolism molecule [10], initiating a cascade that culminates in axon degeneration [11, 12]. Hence, SARM1 is the central executioner of axon degeneration and its deletion confers dramatic resistance to injury-induced axon loss and prevents the development of diverse neuropathies, including models of chemotherapy-induced peripheral neuropathy (CIPN), Charcot-Marie-Tooth (CMT) type 2A, and high fat diet-induced neuropathy [13–15]. We previously developed a mouse model (*Nmnat2*$^{V98M/R232Q}$ mice) of a human congenital neuropathy disorder caused by compound heterozygosity of two different Nmnat2 missense variants [2]. These mice exhibit chronic SARM1 activation in axons due to NMNAT2 enzymatic deficiency, termed "sarmopathy", and recapitulate most of the clinical features and disease progression observed in the patients, including behavioral and electrophysiological deficits, axon loss, and muscle wasting [2]. As anticipated, axon degeneration in this model is driven by chronic activation of SARM1 in the axons, as demonstrated by an increase of the SARM1-specific biomarker, cyclic ADP ribose (cADPR), and the complete rescue of all phenotypes when combined with SARM1 knockout. Disease progression in this model was attenuated by intrathecal administration of adeno-associated virus (AAV) driving neuronal expression of a SARM1 dominant-negative (SARM1-DN) mutant, indicating these phenotypes require SARM1 activity in neurons [2].

Neuroinflammation plays a paramount role in many neurodegenerative diseases, influencing progression and severity [16]. While neuroinflammatory signals can stimulate immune cell recruitment and debris clearance to promote repair and regrowth [16], they also drive disease progression in neurodegenerative conditions such as Alzheimer's Disease (AD), amyotrophic lateral sclerosis (ALS), and multiple sclerosis (MS) [17]. In AD, microglia initially act to contain disease-associated plaques and delay disease progression, but overactivation of microglia can exacerbate disease pathology by damaging neurons through excessive phagocytosis and pro-inflammatory cytokine production [18, 19]. ALS exhibits a similar pattern, with microglia in the spinal cord transitioning from a beneficial role to a neurotoxic phenotype as the disease progresses [20]. In the peripheral nervous system (PNS), macrophages promote nerve regeneration post-injury by removing axonal debris [21], but also contribute to disease pathogenesis in CIPN and aging-related peripheral neuropathy [22–24]. Our previous study identified heightened macrophage activation in sarmopathic peripheral nerves, akin to observations in AD, ALS, and other peripheral neuropathy models [2, 17–20, 22–24]. Notably, macrophage depletion delayed axon loss and reversed motor function deficits in *Nmnat2*$^{V98M/R232Q}$ mice, revealing SARM1-dependent neuroimmune mechanisms as key drivers of the disease.

To seek further insight into the changes in cellular composition and altered gene expression in this condition, we used single cell and single nucleus RNA-sequencing (sc/snRNA-seq) to examine the transcriptome of *Nmnat2*$^{V98M/R232Q}$ peripheral nerves. Similar analyses have reshaped our understanding of the role of disease-associated microglia (DAM) in AD progression [25]. In the PNS, single cell transcriptional characterization revealed microglial activation-associated genes expressed in peripheral nerve macrophages [26], a novel motor-selective myelinating Schwann cell (mSC) subtype [27], and heterogeneity of the nerve cellular components and their response to acute nerve injury [28–30]. From our transcriptome analyses, we identified changes that highlight increased immune-related functions of sarmopathic nerve-resident cells, including endoneurial fibroblasts and Schwann cells (SCs). Chronic SARM1 activation in axons triggers a response from several cell types inducing cytokine and complement production that likely enhance the recruitment and activation of immune cells. Additionally, we identified an expanded $Il1b^+$ macrophage subpopulation that markedly expresses phagocytic and T cell proliferation/activation markers and showed, via in vivo depletion, that T cells contribute to sarmopathic neuropathy progression. Our study thus provides a comprehensive overview of the transcriptional landscape of a chronic SARM1 activation disorder, highlighting the involvement of multiple nerve cell types in provoking an immune response that could be an important target for treating such neurodegenerative diseases.

Results

Sc/snRNA-seq reveals immune cell and repair schwann cell expansions and transcriptional alterations in non-immune nerve-resident cells in *Nmnat2*$^{V98M/R232Q}$ sarmopathy mice

To elucidate tissue-wide responses to chronic SARM1 activation and the mechanisms of SARM1-dependent non-cell-autonomous immune responses, we used sc/snRNA-seq to compare sciatic nerves from wildtype

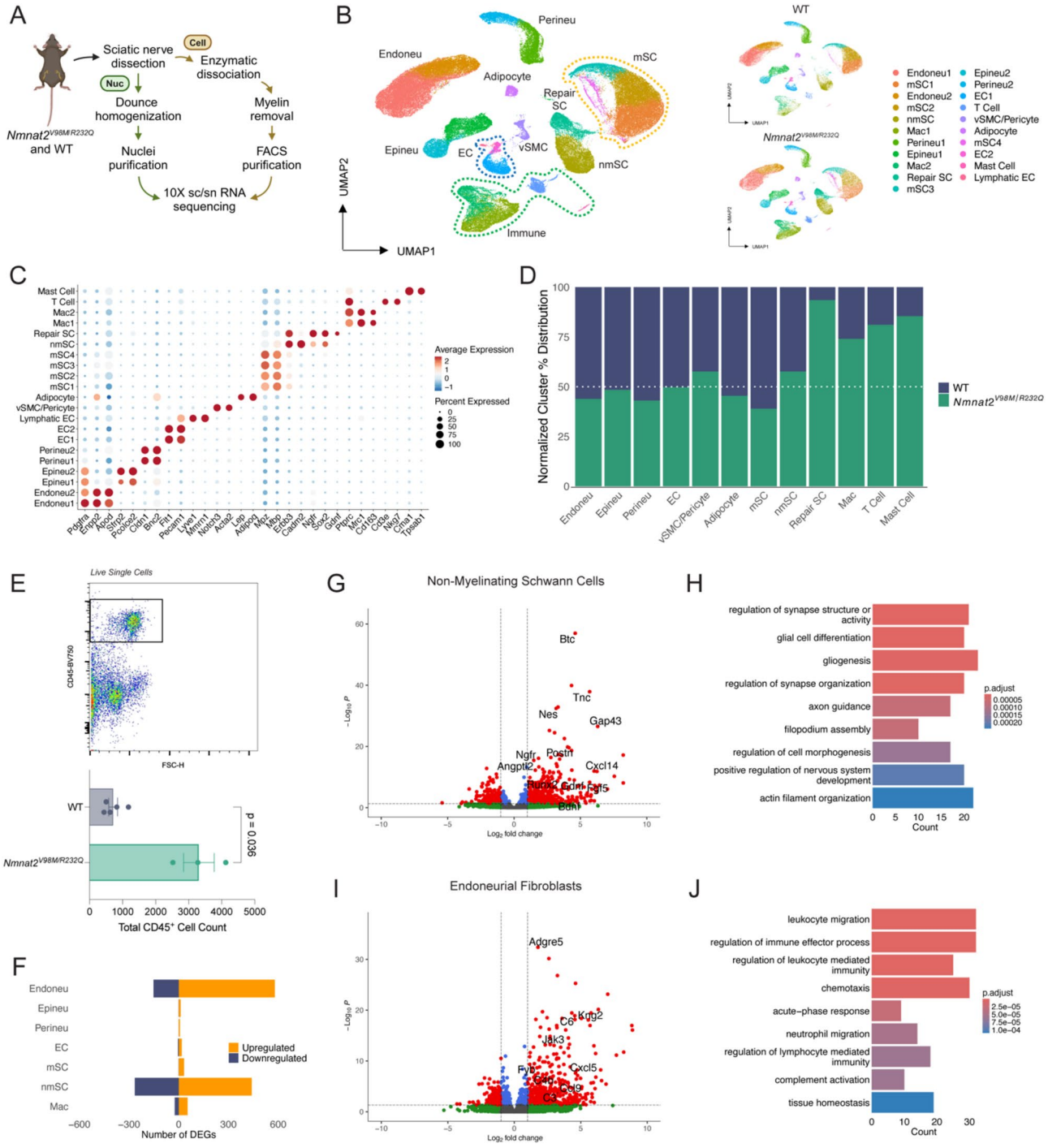

Fig. 1 (See legend on next page.)

(WT) mice to those from our *Nmnat2*$^{V98M/R232Q}$ sarmopathy model. Combining single cell and single nucleus approaches minimized method-dependent differences in cell type recovery, an important consideration in peripheral nerve containing myelinating glia and immune cells [31, 32]. We studied 2-3-month-old mice because, at this age, the sarmopathic mice show abundant activated CD68^{+} macrophages in their nerves and motor behavioral deficits in the absence of significant axon degeneration, indicating a state of early neuroimmune response before irreparable axonal damage has occurred [2]. By focusing on this early stage, we aimed to gain insights into the initiating events that could inform strategies to prevent axon degeneration before its onset.

Our combined approach yielded 101,263 cells/nuclei isolated from sciatic nerves of WT and sarmopathic mice

(See figure on previous page.)

Fig. 1 sc/snRNA-seq of *Nmnat2*$^{V98M/R232Q}$ sciatic nerves reveals immune cell expansions and transcriptomic alterations in nerve-resident cells. (**A**) Schematic of sc/snRNA-seq experimental workflow for 2-3-month-old WT (C57BL/6) and *Nmnat2*$^{V98M/R232Q}$ mice. (**B**) Integrated UMAP visualization of cells from WT and *Nmnat2*$^{V98M/R232Q}$ sciatic nerves ($n = 101,263$; single cell = 42,984; single nucleus = 58,279) and UMAP visualization of WT ($n = 48,785$) and *Nmnat2*$^{V98M/R232Q}$ ($n = 52,478$) side-by-side. Colors correspond to different cell clusters. Endoneu, endoneurial fibroblast; Epineu, epineurial fibroblast; perineu, perineurial fibroblast; EC, endothelial cell; vSMC/pericyte: vascular smooth muscle cell and pericyte; mSC, myelinating Schwann cell; nmSC, non-myelinating Schwann cell; repair SC, repair Schwann cell; Mac, macrophage. (**C**) Dot plot of scaled average canonical marker gene expression used to differentiate and classify cell clusters. (**D**) Stacked bar plot of normalized cell type proportions in WT and *Nmnat2*$^{V98M/R232Q}$. Data was normalized to account for the difference in the total cell count (cluster cell count / normalization factor, where normalization factor = total cell count / largest total cell count). (**E**) Flow cytometry quantification of total number of live single CD45$^+$ immune cells in WT and *Nmnat2*$^{V98M/R232Q}$ sciatic nerves. Data are presented as mean ± SEM. Significance was determined using Mann-Whitney test. (**F**) Number of genes with significantly increased or decreased expression ($\log_2$FC >|1| and adjusted *p*-value < 0.05) per major cell type in *Nmnat2*$^{V98M/R232Q}$ compared to WT nerves. (**G**) Volcano plot and (**H**) Gene Ontology (GO) terms of differentially expressed genes (DEGs) in non-myelinating SCs in *Nmnat2*$^{V98M/R232Q}$ compared to WT. (**I**) Volcano plot and (**J**) GO terms of DEGs in endoneurial fibroblasts in *Nmnat2*$^{V98M/R232Q}$ compared to WT. DEGs with $\log_2$FC > 1 and adjusted *p*-value < 0.05 were used for volcano plot visualization and GO term analysis

(42,984 cells and 58,279 nuclei) (Fig. 1A). Data integration and unsupervised clustering revealed 21 distinct cell clusters consistent with previous sc/snRNA-seq studies of peripheral nerves, including fibroblasts (endoneurial, perineurial, and epineurial), endothelial cells, SCs (myelinating, non-myelinating, and repair), and immune cells (macrophages, T cells, and mast cells) (Fig. 1B) [27, 30]. In particular, our analysis captured populations of repair Schwann cells (repair SCs) and T cells not typically observed in healthy peripheral nerves [27], but consistent with scRNA-seq observations of acute nerve injury [30]. Cell types were defined using well-established canonical cell markers from recent literature (Fig. 1C) [27, 28, 30].

Consistent with our previous flow cytometry study which showed an expansion of CD64$^+$ CD11b$^+$ macrophages [2], sc/snRNA-seq analysis revealed a noteworthy expansion of macrophages in sarmopathic nerves (Fig. 1D). Additionally, we observed a considerable expansion of T cells (Fig. 1D). We validated the increase in total immune cells using flow cytometry analysis of CD45$^+$ cells (Fig. 1E). These results demonstrate that chronic SARM1 activation leads to an increase of immune cells in the nerve, particularly T lymphocytes and macrophages, highlighting the immune cell-enriched composition of sarmopathic nerves as early as two months of age.

We hypothesized that axon distress caused by chronic SARM1 activation could influence gene expression across multiple nerve cell populations. To test this, we performed pseudo-bulk DESeq2 differential gene expression analysis comparing gene expression patterns in the major cell types between WT and *Nmnat2*$^{V98M/R232Q}$ (Supplementary Datasets 1). This analysis revealed a significant number of differentially expressed genes (DEGs), with the most prominent changes observed in non-myelinating Schwann cells (nmSCs) (440 increased and 265 decreased DEGs), and in endoneurial fibroblasts present in the extracellular matrix in close proximity to SC-ensheathed axons (579 increased and 152 decreased DEGs) and (Fig. 1F). While other nerve cell populations such as mSCs, endothelial cells, and macrophages also showed DEGs, endoneurial fibroblasts and nmSCs emerged as the cells with the broadest response to compromised axons. The overall changes observed were confirmed by analysis of our previously published bulk RNA-seq of 2-3-month-old sciatic nerves [2]. In addition, we included bulk RNA-seq of 2-3-month-old *Nmnat2*$^{V98M/R232Q}$;*Sarm1-KO* sciatic nerves to examine the SARM1-dependent nature of the observed transcriptional changes. When compared to WT sciatic nerve, we found negligible differences in the overall transcriptional profiles of *Nmnat2*$^{V98M/R232Q}$ nerves in the absence of SARM1, demonstrating that SARM1 activation in axons, rather than low NMNAT2 activity in non-neuronal cells, is the primary driver of the dramatic changes in gene expression observed in the broad range of nerve cell types (Fig. 1F; Supplementary Fig. 1).

After nerve injury, SCs undergo a de-differentiation process to become repair SCs, a specialized pro-regenerative SC population that supports axon growth and neuronal survival [33]. We suspected that the high number of DEGs associated with sarmopathic nmSCs could be due to inclusion of SCs transitioning into this repair phenotype in response to axonal stress from chronic SARM1 activation. Indeed, we observed a considerable expansion of the repair SC subcluster – defined by high *Ngfr*, *Sox2*, and *Gdnf* expression – in sarmopathic nerves, similar to observations in acute nerve injury models (Fig. 1C and D) [30]. Such transitional SCs downregulate the myelin genes (*Mpz* and *Mbp*) that define mSCs while retaining other SC-associated markers [33]. Thus, DEGs of sarmopathic nmSCs also include repair-associated genes such as *Bdnf*, which enhances nerve regeneration through activation of the JAK/STAT pathway in SCs [34], and *Runx2*, which regulates SC migration and re-myelination during peripheral nerve repair (Fig. 1G) [35]. Significantly increased genes in sarmopathic nmSCs were associated with axon-plasticity, regeneration, and development-related Gene Ontology (GO) terms (Fig. 1H). This supports the interpretation that our analysis has captured a subset of SCs in a transitional repair-like state in response to chronic SARM1 activation and axon distress [36].

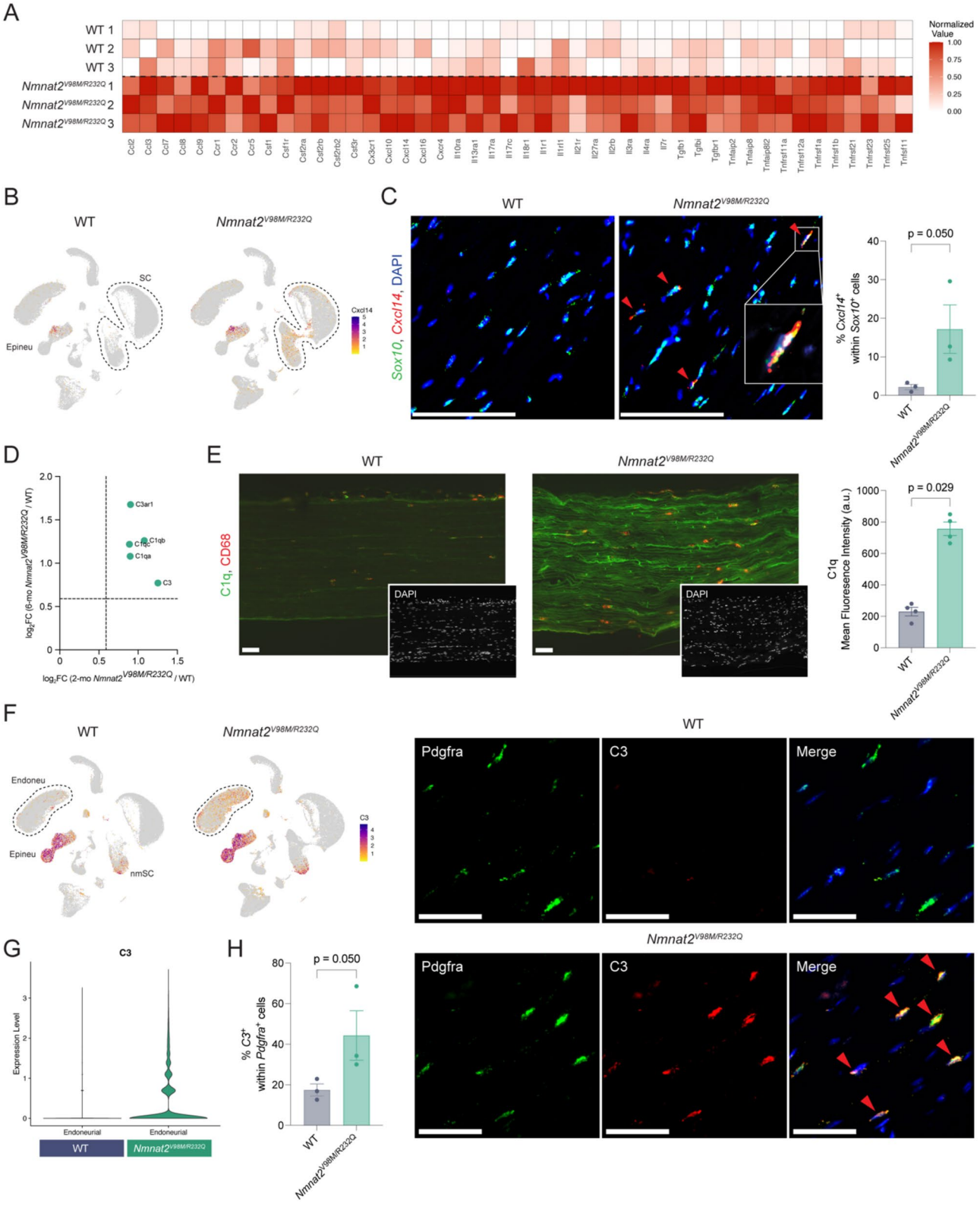

Fig. 2 (See legend on next page.)

(See figure on previous page.)

Fig. 2 Chronic SARM1 activation induces expression of cytokines and complement in nerve-resident cells of *Nmnat2*$^{V98M/R232Q}$ mice. (**A**) Heatmap of normalized cytokine and chemokine mRNA value in bulk RNA-seq data from 2-3-month-old WT and *Nmnat2*$^{V98M/R232Q}$ mice (3 replicates per condition). Color scale normalized by the highest and the lowest expressions across each cytokine. (**B**) UMAP of scaled *Cxcl14* mRNA expression in sc/snRNA-seq of WT and *Nmnat2*$^{V98M/R232Q}$ nerves. (**C**) Representative RNA FISH images and percentage quantification of *Sox10* and *Cxcl14* in 2-3-month-old WT and *Nmnat2*$^{V98M/R232Q}$ sciatic nerves ($n = 3$ per genotype). Scale bar: 100 µm. Data presented as mean ± SEM. Significance was determined using Mann-Whitney test. (**D**) Fold change in complement related bulk mRNA expression in 2-month-old and 6-month-old *Nmnat2*$^{V98M/R232Q}$ sciatic nerves compared to WT ($n = 3$ per condition). (**E**) Representative images and mean fluorescence intensity (MFI) quantification of CD68 (activated macrophages) and C1q (C1q complement components) immunofluorescence in sciatic nerves of 2-3-month-old WT and *Nmnat2*$^{V98M/R232Q}$ mice. Inset shows DAPI (nuclei) staining for same images. Scale bar: 50 µm. Data presented as mean ± SEM. Significance was determined using Mann-Whitney test. (**F**) UMAP of scaled *C3* mRNA expression in sc/snRNA-seq of WT and *Nmnat2*$^{V98M/R232Q}$. (**G**) Violin plot of *C3* mRNA expression in sc/snRNA-seq of WT and *Nmnat2*$^{V98M/R232Q}$ endoneurial fibroblasts. (**H**) Representative RNA FISH images and percentage quantification of *Pdgfra* (green) and *C3* (red), merged with DAPI (blue) in 2-3-month-old WT and *Nmnat2*$^{V98M/R232Q}$ sciatic nerves ($n = 3$ per genotype). Scale bar: 50 µm. Data presented as mean ± SEM. Significance was determined using Mann-Whitney test

In peripheral nerves, Pdgfra$^+$ fibroblasts reside within the nerve endoneurium, near to the S100b$^+$ SCs that ensheathe and myelinate the axons [37]. Fibroblasts are well recognized for their role in regulating tissue immune responses during injury or disease via induction of genes encoding cytokines and other immune-modulating proteins [38–41]. Consistent with this role, we observed increased expression of inflammation and immune recruitment-related genes in sarmopathic endoneurial fibroblasts (Fig. 1I). GO analysis confirmed the enrichment of these DEGs for immune response regulation (Fig. 1J), suggesting immune-enhancing capabilities of endoneurial fibroblasts in response to chronic SARM1 activation. Interestingly, other nerve fibroblasts show a much-reduced transcriptional response to these unhealthy axons, suggesting that the proximity of endoneurial fibroblasts to SC-ensheathed axons allows them to respond to axonal stress and contributes to their enhanced responsiveness. These DEGs include *Kng2*, which supports inflammation during sepsis [42], and the chemokines *Ccl9* and *Cxcl5*, which recruit various immune cells [43–45]. Additionally, *Adgre5/CD97*, a leukocyte adhesion marker that acts to enhance immune cell infiltration and immune microenvironment changes associated with cancer, was also increased [46–48]. Furthermore, the gene encoding FYB/ADAP—critical for T cell activation and chemokine signal transduction—was increased in sarmopathic endoneurial fibroblasts (Fig. 1I) [49]. Similar immune regulation and immune cell signaling related gene expression changes were also observed in sarmopathic endothelial cells (Supplementary Fig. 2). Taken together, these results demonstrate that chronic SARM1 activation in peripheral nerves leads to a significant expansion of immune cells (macrophages and T lymphocytes) and repair SCs, and a surprisingly broad transformation of inflammatory gene regulation in a wide range of nerve cell types. This multi-cell type response to chronic axonal SARM1 activation, both in terms of altered cellular composition and transcription, provides new avenues to identify therapeutic strategies.

Chronic SARM1 activation increases expression of cytokines and complement in multiple nerve-resident cell populations

Cytokines and chemokines play a central role in coordinating immune responses, enabling recruitment, activation, and differentiation of immune cells [50, 51]. Re-analysis of our published bulk RNA-seq revealed increased expression of genes encoding cytokines, chemokines, and their receptors, such as *Ccl2*, *Ccl8*, *Cxcl14*, and *Cxcl16*, in sarmopathic nerves (Fig. 2A) [2]. We validated these findings at the protein level using Luminex multiplex assays, which showed positive correlations between mRNA and protein levels (Supplementary Fig. 3A). We then examined our sc/snRNA-seq data to determine the cell types expressing the cytokines and chemokines induced by chronic SARM1 activation (Supplementary Fig. 3B). Notably, *Cxcl14* is expressed in both WT and sarmopathic epineurial fibroblasts but is significantly increased in sarmopathic nmSCs and mSCs (DESeq2 pseudo-bulk differential analysis; nmSC: $\log_2$FC = 6.02, adj p-value = 1.18e-12; mSC: $\log_2$FC = 5.91, adj. p-value = 4.38e-5) (Figs. 1G and 2B). CXCL14 contributes to the regulation of immune cell migration, as demonstrated in a recent glioma study where CXCL14 recruited tumor-infiltrating CD8$^+$ T cells [52, 53]. To mitigate potential gene expression biases from single cell/nuclei mechanical dissociation and enzymatic digestion [54], we validated our findings using RNA fluorescence in situ hybridization (FISH), confirming increased expression of *Cxcl14* in SCs (identified by *Sox10* expression) in sarmopathic sciatic nerves (Fig. 2C). These findings suggest that SCs respond to early axonal distress by de-differentiating to a repair phenotype and recruiting immune cells, including T cells, to the peripheral nerves.

Activation of the complement system is another crucial mechanism guiding recruitment and regulation of the immune response and directing cell destruction. Overactivation of the complement cascade leads to neuroinflammation, synaptic dysfunction, and neuronal death, contributing to the progression of many neurodegenerative diseases including AD, ALS, and MS [55–58]. In the PNS, activation of the complement cascade has

been observed in myasthenia gravis, where pathological destruction of the neuromuscular junction is primarily driven by complement-mediated lysis of the postsynaptic membrane [59, 60]. Similar observations have been made in acute sciatic nerve ligation and CIPN models, where complement inhibition suppressed the infiltration of inflammatory immune cells and attenuated axon loss, respectively [61, 62]. Analysis of bulk RNA-seq of sciatic nerves from 2- and 6-month-old *Nmnat2*$^{V98M/R232Q}$ mice revealed a significant increase in expression of complement-related genes such as *C3* (the central component of the complement cascade essential for amplifying the complement response), *C1qa/b/c* (parts of the C1 complex responsible for recognizing antigen-antibody complexes), and complement receptor *C3ar1* (which binds complement peptide C3a) (Fig. 2D) [2, 63, 64]. We used immunohistochemistry to confirm the increased expression of C1q—the recognition subunit of the first complement component that initiates the classical complement pathway—and observed its deposition on SCs ensheathing axons (Fig. 2E) [63]. Consistent with previous findings, we confirmed that *C1qa/b/c* are synthesized by macrophages in our dataset (Supplementary Fig. 4) [65]. Our sc/snRNA-seq data showed high basal expression of *C3* in epineurial fibroblasts in both WT and sarmopathic nerves. Additionally, we found *C3* expression significantly induced in the endoneurial fibroblasts in sarmopathic nerves (DESeq2 pseudo-bulk differential analysis; endoneurial fibroblast: $\log_2$FC = 3.27, adj *p*-value = 0.0001) (Figs. 1I and 2F and G). RNA FISH confirmed the increase of *C3* expression in sarmopathic nerves and demonstrated its co-expression with *Pdgfra*, a marker of fibroblasts (Fig. 2H). The increased *C3* expression in sarmopathic nerves suggests activation of the complement system similar to other neurodegenerative diseases, particularly driven by an endoneurial fibroblast response to chronic SARM1 activation in the axons.

In summary, our findings demonstrate and validate the induction of immune-related genes in non-immune nerve-resident cells within sarmopathic nerves. Our model suggests that SCs and endoneurial fibroblasts sense SARM1-induced microenvironment changes in the axon and adopt immune-related functions i.e. secretion of pro-inflammatory cytokines and complement components. These factors recruit and activate immune cells, likely amplifying neuroinflammatory responses to persistent SARM1 activation in axons.

Il1b$^+$ macrophages with elevated phagocytosis and T cell proliferation/activation functions are abundant in sarmopathic nerves

The expansion of multiple immune cell types in our sc/snRNA-seq data, coupled with the increased expression of cytokines and complement components, prompted us to further refine the immune cell subclusters identified in the nerves. We previously showed that PNS macrophages share a significant overlap in gene expression with CNS microglia in a healthy state, including expression of microglial activation genes [26]. In AD, a subset of microglia known as DAM is prevalent at sites of neurodegeneration, exhibiting unique functions and pathways associated with pathology [25]. Linking these observations in the context of peripheral neurodegeneration, we hypothesized that a unique subset of macrophages is expanded in sarmopathic nerves. While our previous study demonstrated the role of macrophages in driving SARM1-dependent inflammatory neuropathy, our understanding of the responsible macrophage subtype remains limited. To test this hypothesis, we performed fluorescence-activated cell sorted (FACS) scRNA-seq on CD45$^+$ immune cells from sciatic nerves of 2-3-month-old sarmopathic mice. Combining our CD45$^+$ sorted single cell data with immune cell subclusters from the scRNA-seq dataset (Fig. 1A), we captured and analyzed 10,140 immune cells: 7,125 from *Nmnat2*$^{V98M/R232Q}$ and 3,015 from WT (Fig. 3A). Unsupervised clustering of the immune cells revealed five macrophage clusters (Myo5a$^+$, Ccl3$^+$, Clta$^+$, Il1b$^+$, Ccl9$^+$), four T cell clusters (T, Cytotoxic T/NK, Helper T, Gamma Delta T), monocytes, B cells, dendritic cells, mast cells, and neutrophils. Cell populations were defined using canonical markers for each immune cell type from recent literature (Fig. 3B) [27, 30, 66–68]. Consistent with our sc/snRNA-seq analysis, we observed a significant increase in the total number of macrophages, as well as T cells, B cells, and dendritic cells, in the sarmopathic nerves even at this early stage of the disease (Fig. 3C) [2]. Among the five distinct macrophage clusters, the Il1b$^+$ macrophage subpopulation alone showed a significant increase in its proportional distribution (Fig. 3D; Supplementary Fig. 5).

Macrophages that highly express *Il1b* amplify inflammation in various diseases such as pancreatic ductal adenocarcinoma (PDAC) and inflammatory arthritis (IA) [69, 70]. In our model, the macrophage subcluster highly expressing *Il1b* (Fig. 3E) also selectively expressed genes related to inflammation (*Chil3*, *Thbs1*, *Sirpb1c*, *Tyrobp*), phagocytosis (*Cd300a*), and T cell proliferation/activation (*Cd44*, *Klra2)* (Fig. 3F). Many of the increased inflammation genes in sarmopathic Il1b$^+$ macrophages were also found to be elevated in Il1b$^+$ macrophages identified in PDAC, such as *Plac8*, *Thbs1*, *Vcan*, *Flt1*, *Trem1*, and *Arg2* (Supplementary Datasets 2) [69]. Additionally, genes typically associated with DAMs, including *Lgals3*, *Tyrobp*, *Cebpb*, *B2m*, *Lyz2*, and *H2-D1*, were increased in these Il1b$^+$ macrophages (Supplementary Fig. 6) [25]. Flow cytometry confirmed the significantly increased expression of IL1b in sarmopathic macrophages (CD45$^+$ CD11b$^+$ F4/80$^+$ Ly6C^{low}) (Fig. 3G). GO

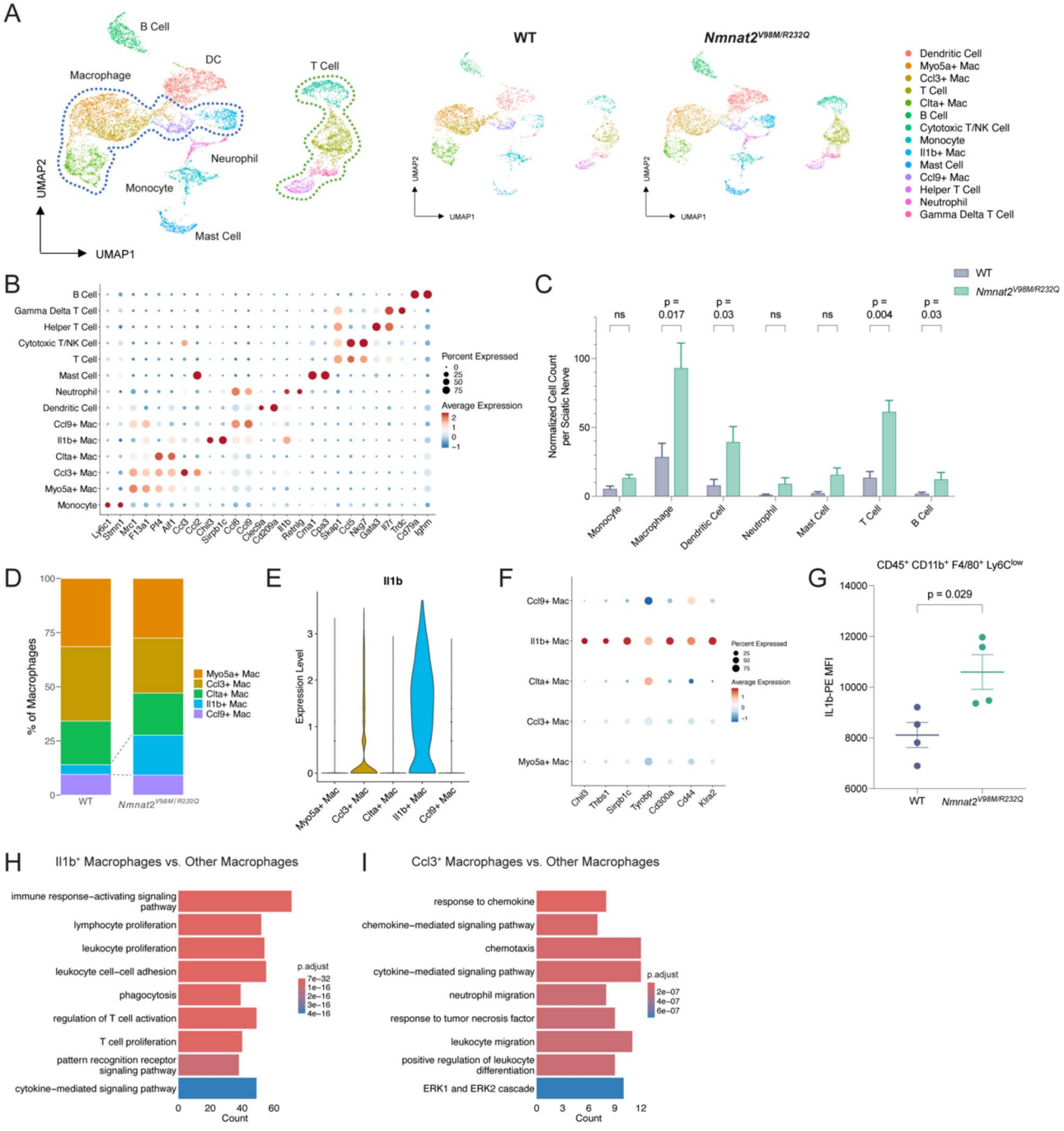

Fig. 3 Analysis of CD45$^+$ immune cells reveals expansion of Il1b$^+$ macrophages in *Nmnat2*$^{V98M/R232Q}$ nerves. (**A**) Integrated UMAP visualization of CD45$^+$ immune cells from WT and *Nmnat2*$^{V98M/R232Q}$ sciatic nerves ($n = 10{,}140$ cells) and side-by-side UMAP visualization of WT ($n = 3{,}015$) and *Nmnat2*$^{V98M/R232Q}$ ($n = 7{,}125$). The immune cell subclusters from scRNA-seq are integrated with FACS CD45$^+$ scRNA-seq data. Colors correspond to different cell clusters. Mac, macrophage; NK, natural killer cell. (**B**) Dot plot of scaled average canonical marker gene expression used to differentiate and classify immune cell clusters. (**C**) Bar graph of normalized immune cell count accounting for the number of sciatic nerves in each group (normalized cell count = cluster cell count / number of sciatic nerves pooled for the sample). Data presented as mean ± SEM. Significance was determined using Mann-Whitney test. (**D**) Cluster distribution of macrophage (Mac) subclusters in WT and *Nmnat2*$^{V98M/R232Q}$ nerves. (**E**) Violin plot of scaled *Il1b* mRNA expression in macrophage clusters. (**F**) Dot plot illustrating scaled expression of differentially expressed genes in Il1b$^+$ macrophages including inflammation (*Chil3*, *Thbs1*, *Sirpb1c*, *Tyrobp*), phagocytosis related (*Cd300a*), and T cell proliferation/activation related (*Cd44*, *Klra2*) genes. (**G**) Flow cytometry MFI analysis of IL1b expression in CD45$^+$ CD11b$^+$ F4/80$^+$ Ly6C^{low} macrophages in nerves from 2-3-month-old WT and *Nmnat2*$^{V98M/R232Q}$ mice ($n = 4$ per genotype). Data presented as mean ± SEM. Significance was determined using Mann-Whitney test. (**H**) Enriched Gene Ontology (GO) terms associated with Il1b$^+$ macrophages or (**I**) Ccl3$^+$ macrophages compared to other macrophage populations. DEGs with $\log_2$FC > 1 and adjusted *p*-value < 0.05 were used for GO term analysis

analysis of the genes increased in sarmopathic Il1b$^+$ macrophages compared to the other macrophage subclusters suggested enhanced phagocytosis and T cell proliferation/activation functions (Fig. 3H). In contrast, the Ccl3$^+$ macrophage cluster—which is proportionally reduced in sarmopathic nerves—was characterized by increased expression of chemotaxis and immune cell migration-related genes (Fig. 3I).

We identified a unique Il1b$^+$ macrophage population, enriched in phagocytosis and T cell proliferation/activation markers, that is selectively expanded in sarmopathic nerves. This finding suggests that macrophages in SARM1-activated nerves shift toward a more pro-inflammatory state (Il1b$^+$), dedicated to phagocytic debris removal and induction of T cell proliferation and activation. Conversely, the relative decrease in the proportion of Ccl3$^+$ macrophages indicates a shift away from general immune cell recruitment, possibly due to this task being assumed by non-immune tissue-resident cells, as highlighted. The significant expansion of these Il1b$^+$ macrophages with strong inflammatory signatures suggests that they act as key drivers of neuroinflammation and thus disease progression.

Increased numbers of T lymphocytes are present in sarmopathic nerves

In addition to microglia/macrophages, T lymphocytes are implicated in driving inflammation and contributing to neuronal loss in neurodegenerative diseases including AD, MS, and Parkinson's Disease (PD) [71–75]. Infiltration of T cells occurs in both the cerebrospinal fluid and hippocampus of patients with AD [76, 77]. Similarly, CD8$^+$ and CD4$^+$ T cells contribute to the pathogenesis of inflammatory neuropathies, such as chronic inflammatory demyelinating polyradiculopathy (CIDP) and Guillain-Barre syndrome (GBS) [78–80]. Drawing parallels between these inflammatory neuropathies and our *Nmnat2*$^{V98M/R232Q}$ model, we hypothesized that T cells participate in the deficits resulting from chronic SARM1 activation. Consistent with the observed expansion of T cells in our single cell analysis, immunostaining of 2-3-month-old sarmopathic femoral nerves revealed increased expression of pan-T cell (CD3), helper T cell (CD4), and cytotoxic T cell (CD8) markers (Fig. 4A) [71]. Corresponding to the increase in cytotoxic T cells, we observed increased granzyme B expression, which is released by activated cytotoxic T cells and natural killer cells to mediate neurotoxicity (Fig. 4A) [81]. Additionally, we observed an increase in major histocompatibility complex class II (MHC-II) expression by antigen-presenting cells (APCs; macrophages and dendritic cells), which is important for T cell recruitment and for initiating helper T cell responses (Fig. 4A; Supplementary Fig. 7) [82]. The upregulation of MHC-II indicates increased presence of APCs and presumably enhanced antigen presentation capabilities, potentially facilitating sustained T cell activation in sarmopathic nerves and promoting axon destruction.

Corroborating our immunostaining results, flow cytometry quantification confirmed a significant increase in T cells and macrophages in 2-3-month-old sarmopathic sciatic nerves. A trend towards increased dendritic cells was observed but was not statistically significant (Fig. 4B). Collectively, our findings demonstrate a significant expansion of T cells in sarmopathic peripheral nerves. This T cell infiltration, coupled with increased MHC-II expression and the expansion of sarmopathic Il1b$^+$ macrophages enriched in T cell proliferation and activation functions, suggests a coordinated adaptive and innate immune response driving SARM1-dependent neuroinflammation.

T cell depletion improves motor function and reduces axon loss in *Nmnat2*$^{V98M/R232Q}$ Mice

The increased number of T cells in sarmopathic nerves prompted us to investigate their role in disease pathology. To evaluate this, sarmopathic mice were intraperitoneally injected with a T cell depletion cocktail (anti-CD4 and anti-CD8 neutralizing antibodies) or isotype control (IgG antibody). The injections were administered weekly for three months, starting at two months of age—a critical intervention timepoint when inflammatory responses are prevalent but axon degeneration is not yet observed (Fig. 5A) [2]. The efficacy of T cell depletion was confirmed using flow cytometry, which showed strong depletion of CD8$^+$ and CD4$^+$ T cells in sarmopathic sciatic nerves after three months of treatment (Supplementary Fig. 8).

Notably, sarmopathic mice treated with the T cell depletion strategy showed significant improvements in motor function and muscle strength compared to those treated with IgG, which continued to exhibit decreased motor function (Fig. 5B). Morphological examination of the predominantly-motor femoral nerves post-treatment showed significantly reduced axon loss in T cell-depleted mice compared to IgG-treated controls (Fig. 5C and D). These findings of functional and morphological improvement upon T cell depletion demonstrate that T cells contribute to axon degeneration and dysfunction in our sarmopathy model. Upon T cell depletion, we also observed a two-fold decrease in the total number of macrophages in the femoral nerve of *Nmnat2*$^{V98M/R232Q}$ mice compared to IgG-treated controls (Fig. 5E). Furthermore, the number of activated CD68$^+$ macrophages in the femoral nerves of T cell-depleted *Nmnat2*$^{V98M/R232Q}$ mice was reduced (Fig. 5E). This reduction in activated macrophages likely contributes to the observed neuroprotection, paralleling the outcomes observed with macrophage

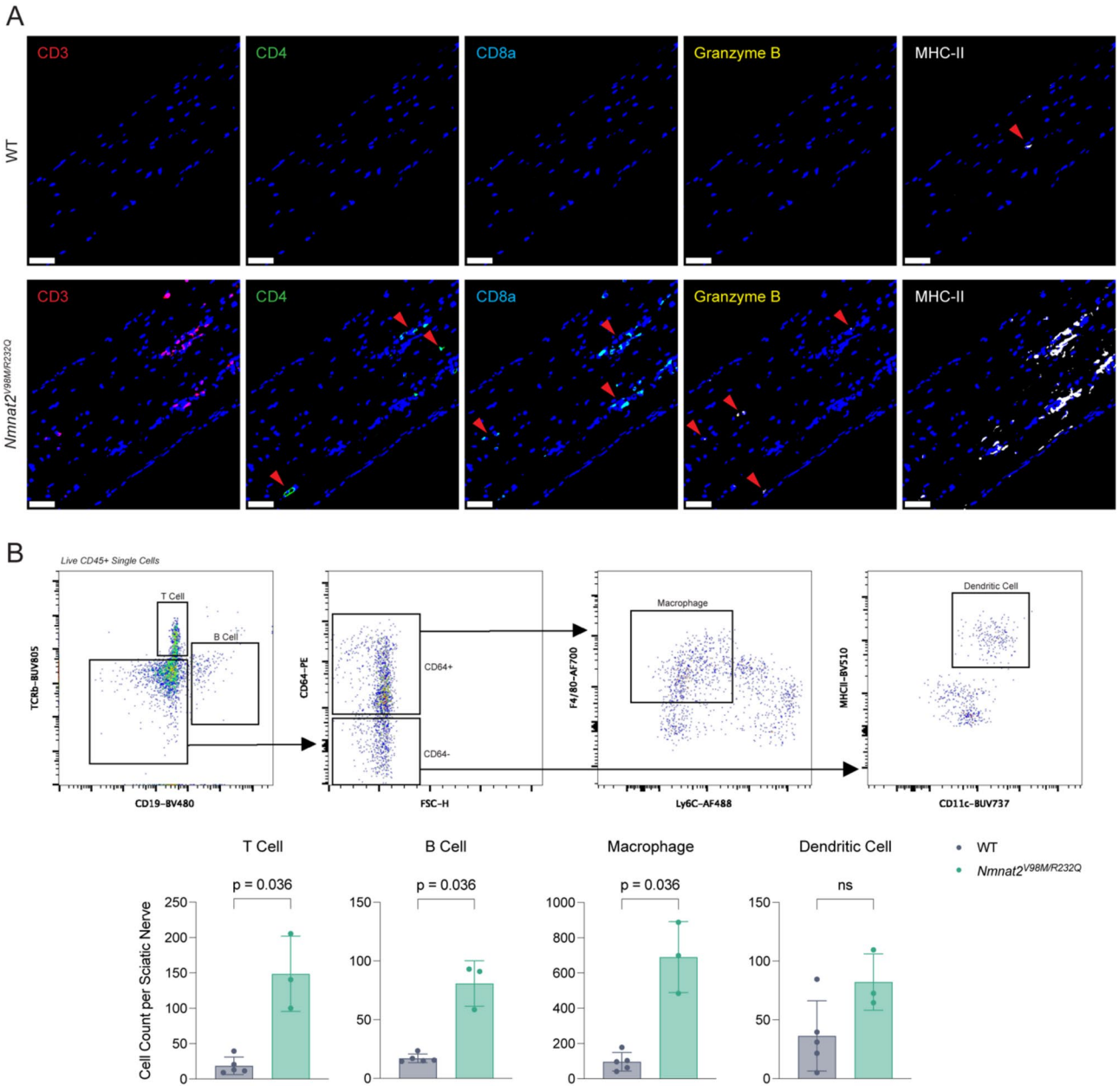

Fig. 4 T lymphocytes are increased in peripheral nerves of *Nmnat2*$^{V98M/R232Q}$ mice. (**A**) Representative images of CD3, CD4, CD8a, granzyme B, and MHC-II immunofluorescence of 2-3-month-old WT and *Nmnat2*$^{V98M/R232Q}$ femoral nerves using PhenoCycler-Fusion multiplexed imaging. Scale bar: 50 µm. (**B**) Flow cytometry gating strategy and quantification of live adaptive immune cells (T cells and B cells) and antigen presenting cells (macrophages and dendritic cells) in 2-3-month-old WT and *Nmnat2*$^{V98M/R232Q}$ sciatic nerves. Each dot in the graph corresponds to an individual sciatic nerve. Data are presented as mean ± SEM. Significance was determined using Mann-Whitney test

depletion via CSF1R-antibody treatment [2], underscoring the complexity of the neuroimmune response and the contribution of multiple immune cell types in driving neuroinflammation and disease progression in SARM1-dependent neuropathy.

Discussion

Neuroinflammation, a central component of neurodegenerative disease, arises from the immune response to injury that eliminates dead or dying cells and initiates healing [16]. This process includes the production of cytokines, chemokines, reactive oxygen species, and secondary messengers, predominantly by glial and immune cells [83, 84]. We previously observed abundant activated macrophages, a key constituent of the

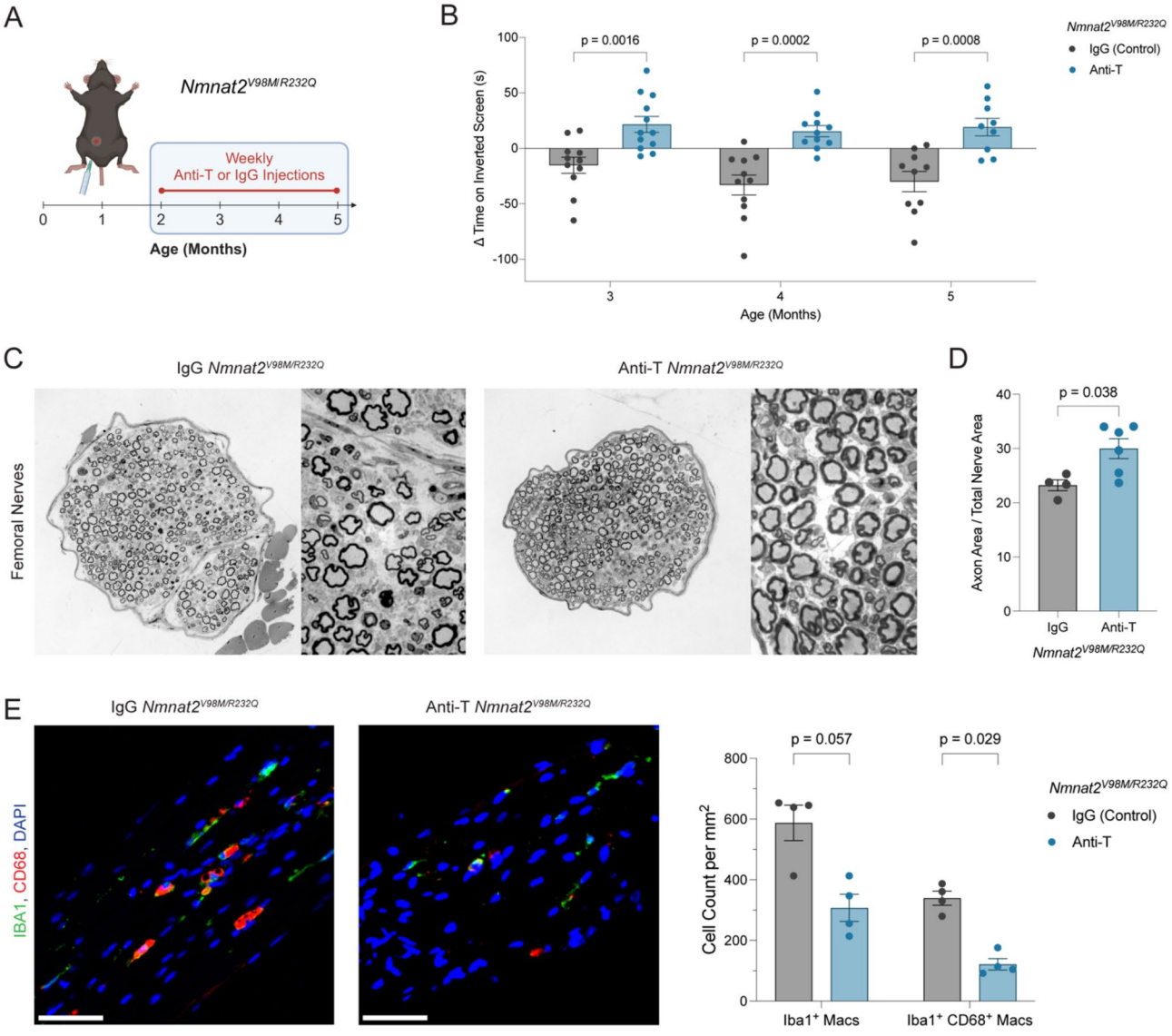

Fig. 5 T cell depletion in *Nmnat2*$^{V98M/R232Q}$ mice prevents motor deficits and femoral axon loss. (**A**) Schematic of T cell depletion experimental workflow in *Nmnat2*$^{V98M/R232Q}$ mice. Mice were injected with anti-CD4 & anti-CD8 neutralizing antibodies ($n=10$) or IgG control ($n=12$) weekly from two to five months of age. Two months-old was selected as a critical intervention timepoint prior to axon loss but after onset of neuroinflammation. (**B**) Changes in motor function of IgG-treated ($n=10$) and T cell-depleted *Nmnat2*$^{V98M/R232Q}$ mice ($n=12$) from three months to five months measured as changes in inverted screen latency time to fall compared to the baseline measurement for each mouse prior to treatment at two months. Data are presented as mean ± SEM. Significance was determined using mixed-effects analysis with Geisser-Greenhouse correction and Sidak's multiple comparisons. (**C**) Representative images of femoral nerves from IgG-treated and T cell-depleted *Nmnat2*$^{V98M/R232Q}$ mice at five months at 20X and 100X magnification. (**D**) Percent axonal area/total nerve area for femoral nerves calculated at five months after three months of T cell depletion ($n=6$) or treatment with IgG control ($n=4$). Data presented as mean ± SEM. Significance was determined using Mann-Whitney test. (**E**) Representative images and quantification of Iba1$^+$ and CD68$^+$ macrophages of femoral nerves in IgG control and T cell-depleted *Nmnat2*$^{V98M/R232Q}$ nerves at five months ($n=4$). Scale bar: 50 µm. Data presented as mean ± SEM. Significance was determined using Mann-Whitney test

neuroinflammatory response, at an early stage of phenotypic progression in our model of *sarmopathy*. In this model, where pathology is driven by persistent SARM1 activation in axons, we found that depletion of macrophages also significantly delayed motor dysfunction, implying that a non-cell-autonomous mechanism engages macrophages to promote axon degeneration downstream of SARM1 [2]. Indeed, our recent study identified dysregulation of phosphatidylserine (PS), a potent phagocytic "eat me" signal, as an early indicator of axonal stress in sarmopathy [85]. Here, our transcriptional characterization of the sarmopathic nerve reveals processes beyond macrophage activation that drive the pathogenic neuroimmune response in SARM1-dependent inflammatory neuropathy. These include the recruitment of immune cells other than macrophages,

such as T cells, and immune regulation by non-immune nerve-resident cells near sarmopathic axons, namely SCs and endoneurial fibroblasts.

Our sc/snRNA-seq findings revealed significant alterations in both the distribution of nerve cell populations and their transcriptional profiles at an early stage of pathology. These changes were evident prior to observable axon degeneration, indicating a proactive response to chronic SARM1 activation. In addition to immune cell (macrophage and T lymphocyte) expansion, we observed the emergence of repair SCs, historically studied in acute nerve injury models and crucial to peripheral nerve regeneration [33]. Their presence in our chronic early-stage model suggests that a repair signal is present even in the absence of overt axonal damage. The concurrent emergence of repair SC phenotypes and the increase in immune cells early in the disease process likely set the stage for subsequent neuroinflammatory and degenerative processes, highlighting potential early intervention points for SARM1-dependent neuropathy.

Non-immune nerve-resident cells, particularly SCs and endoneurial fibroblasts, appear to act as auxiliary immune mediators, secreting pro-inflammatory cytokines/chemokines and complement components in the sarmopathy model, which aligns with findings from other disease states. For example, tumor-associated fibroblasts attract and maintain macrophages by secreting cytokines and chemokines such as CCL2 and CCL5 [86, 87], and in the CNS, astrocytes produce inflammatory mediators such as IL-1, IL-6, and TNFa in response to neuronal a-synuclein aggregation associated with PD pathogenesis [88]. Furthermore, increased expression of C1q and C3 suggests activation of the complement system through its classical pathway, triggered by recognition of "eat me" signals such as phosphatidylserine [89]. In AD models, complement and microglia mediate early synapse loss, highlighting the potential detrimental effect of complement activation in SARM1-dependent neuropathy [90].

Our findings emphasize the underappreciated role of many nerve cell populations responding to axonal stress. In particular, sarmopathic endoneurial fibroblasts appear to release cytokines, chemokines, and complement components in response to axon stress, shaping the nerve microenvironment through immune cell recruitment and immune response regulation. Similarly, endoneurial fibroblasts in the CMT1X neuropathy model express colony stimulating factor-1 (CSF-1) to locally attract disease-associated macrophages [91]. A deeper understanding of these endoneurial responses, as well as other nerve cell populations, could lead to new therapeutic targets for modulating a detrimental neuroinflammatory environment.

Our scRNA-seq analysis of $CD45^+$ cells in sarmopathic nerves revealed selective expansion of $Il1b^+$ macrophages among the five distinct macrophage subclusters identified. This subcluster exhibits a unique transcriptional profile with a significant enrichment in phagocytosis and T cell proliferation/activation functions. The transcriptional profile of $Il1b^+$ macrophages in sarmopathic nerves is similar to those found in pancreatic cancer associated with inflammatory reprogramming and disease progression, suggesting an exacerbating pro-inflammatory state [69]. Similarly, IL1b release from macrophages has been implicated in vincristine-induced peripheral neuropathy (VIPN), highlighting a critical role of macrophages expressing Il1b in multiple models of peripheral neuropathy [92]. GO analysis of genes expressed more highly in $Il1b^+$ macrophages than in other macrophage subclusters indicates increased phagocytosis and orchestration of T cell proliferation and activation, suggesting mechanisms by which $Il1b^+$ macrophages drive disease. Conversely, GO analysis of the remaining macrophages—such as the $Ccl3^+$ macrophage subcluster that is proportionally reduced in sarmopathic nerves—indicates enrichment of immune cell recruitment functions. We speculate that the proportional decline in macrophages dedicated to immune recruitment may be offset by the upregulation of chemotactic and complement pathways in endoneurial fibroblasts and SCs. As these non-immune nerve-resident cells take on chemotactic signaling roles, macrophages may shift toward a more pro-inflammatory $Il1b^+$ state specialized to perform functions like phagocytosis and antigen presentation. This demonstrates the plasticity of macrophages and other nerve constituents to respond to nerve microenvironment changes created by subacute SARM1 activation.

While considerable progress has been made in elucidating the role of T cells in neuroinflammation and neurodegenerative disease [71, 73, 93–95], their contribution to SARM1-dependent neuropathy was previously unknown. We observed an increase in T cells in sarmopathic nerves, potentially due to the enhanced T cell proliferation function of $Il1b^+$ macrophages. This pattern of macrophage-mediated T cell expansion parallels observations in AD tau pathology, where activated microglia recruit T cells into the brain parenchyma and both cell types contribute to disease progression [71]. Like macrophage depletion [2], T cell depletion improved motor functions and reduced axon loss in motor-dominant femoral nerves. Interestingly, depletion of T cells also resulted in a reduction of $CD68^+$ (activated) macrophages, consistent with the known interplay between innate and adaptive immune responses. These findings indicate that T cells also contribute to non-cell-autonomous axon degeneration in SARM1-induced neuroinflammation, broadening our formerly macrophage-centered conception. Furthermore, this macrophage-T cell synergy is also observed in hereditary neuropathies. Macrophage

proliferation is a common feature in CMT1 models, and targeted macrophage depletion leads to sustained axonopathy improvement [96, 97]. Similarly, in CMT1B mouse models crossed with recombination-activating gene-1 (RAG1)-deficient mutants, reductions in $CD4^+$ and $CD8^+$ T cells correlate with fewer macrophages and marked improvements in demyelination [98]. Additional evidence from other models links T cells to axon degeneration through serine-protease granzyme B. In MS and other brain inflammatory disorders, the release and accumulation of cytotoxic granzyme B from activated T cells induces selective neuronal injury [81, 99]. In demyelinating disorders induced by mutations in *PLP1*, a major myelin protein of the CNS, $CD8^+$ T cells also drive axon degeneration via granzyme B, but target myelinating oligodendrocytes rather than neurons [100]. Aligned with these findings, we observed increased granzyme B deposition in early stage sarmopathic nerves, suggesting that granzyme B released by activated T cells may similarly promote axon degeneration in sarmopathy and potentially in CMT neuropathy.

Ultimately, our findings support a model in which chronic SARM1 activation in axons triggers a cascade of events in peripheral nerves leading to a response encompassing a broad range of cell types. SARM1 activation initially leads to low NAD^+ and metabolic dysfunction in axons, resulting in stressed-but-viable axons. In response, nerve-resident cells undergo significant transcriptional changes, including the initiation of a repair SC program despite the absence of frank axon loss. The cumulative alterations in the microenvironment, likely driven by axonal dysfunction, dysregulation of PS, and the surrounding cell responses, further recruit immune cells to the nerves. This recruitment leads to an expansion of macrophages, particularly $Il1b^+$ macrophages with enhanced phagocytic and T cell proliferation/activation functions. T cell numbers also increase, presumably due to these $Il1b^+$ macrophages, further driving neuroinflammation and axon degeneration, potentially via neurotoxic granzyme B release.

Although our transgenic sarmopathic mouse model recapitulates hereditary motor-dominant inflammatory neuropathy, it remains to be determined whether the same immune cell types—$Il1b^+$ macrophages and T lymphocytes—are increased in the nerves of human patients with chronic SARM1 activation. Promisingly, prior studies demonstrated T cell and macrophage infiltration in CMT1 patient nerves [101], a 25-fold increase in $CD3^+$ T cells in sural nerve biopsies of patients with diabetic peripheral neuropathy [102], and the presence of cytotoxic myelin-reactive $CD4^+$ T cells in the nerves of patients with GBS [80]. Confirming our findings in human patients with chronic SARM1 activation would support the therapeutic targeting of T cells to mitigate non-cell-autonomous axon degeneration, offering a promising therapeutic strategy, either alone or in combination with SARM1 inhibitors, for treating neurodegenerative disease.

Materials and methods

Experimental animals

Mice were housed and used following the institutional animal study guidelines and protocols approved by the Institutional Animal Care and Use Committee of Washington University in St. Louis. Mice were maintained on a 12-hour light-dark cycle and food/water provided ad libitum. Both female and male mice were used for the experiments described in this study.

Tissue dissociation and single cell/nucleus suspension

Single cells

For single cell RNA-sequencing, sciatic nerves from 2 mice were pooled. Mice were euthanized and perfused with ice cold PBS. Nerves were collected and immediately kept on ice in DMEM with 1% FBS, RNase-In RNase inhibitor (Promega N2518), and SUPERase-In RNase Inhibitor (Invitrogen AM2696) at 1:1000 ratio. The nerves were mechanically dissociated with shears and incubated in DMEM with 1% FBS containing collagenase II (4 mg/mL; Worthington Biochemical LS004176) and Dispase II (2 mg/mL; Sigma-Aldrich D4693-1G) at 37˚C for 30 min with gentle shaking. The samples were pipetted up and down at 15 min. The cells were filtered through pre-wet 70-µm cell strainers and washed twice with buffer containing DMEM, 1% FBS, RNase-In, and SUPERase-In. Myelin was removed using Myelin Removal Beads II (Miltenyi Biotec 130-096-731) and LS columns (Miltenyi Biotec 130-042-401) per manufacturer's manuals (Miltenyi Biotec IM0001691). Additional debris and dead cells from the single cell suspensions were excluded by immediate FACS using propidium iodide (PI). Cells were collected into PBS with 10% FBS prior to library preparation. The purified single cells were used to prepare scRNA-seq libraries following the 10X Genomics manufacturer's manuals at the Genome Technology Access Center (GTAC) @ McDonnell Genome Institute (MGI) using 10X Genomics v3.1 chemistry.

Single nuclei

For single nucleus RNA-sequencing, sciatic nerves from 2 mice were pooled. Mice were euthanized and perfused with ice cold PBS. The nerves were collected and immediately flash frozen in dry ice. The nerves were mechanically dissociated with shears in cold lysis buffer containing 10mM Tris buffer, 5mM CaCl2, 3mM $Mg(Ac)_2$, 0.05% CHAPS, 320mM sucrose, 1mM DTT, 5X EDTA-free protease inhibitor (Millipore Sigma 11873580001), RNase-In RNase inhibitor (Promega

N2518), and SUPERase-In RNase Inhibitor (Invitrogen AM2696) at 1:1000 ratio in nuclease-free water. The samples were transferred into a glass Dounce homogenizer on ice and mechanically dounced with 10 loose strokes and 20 tight strokes. The samples were filtered through a pre-wet 40-µm cell strainer (Fisher Scientific MT4040) and washed twice with cold wash buffer containing PBS, 0.1% BSA, RNase-In, and SUPERase-In. After removing the supernatant, the nuclear pellet was washed with 3mL of cold wash buffer. The samples were further purified using Anti-Nucleus MicroBeads (Miltenyi Biotec 130-132-997) per manufacturer's manuals. The purified single nuclei were used to prepare snRNA-seq libraries following the 10X Genomics manufacturer's manuals at the Genome Technology Access Center (GTAC) @ McDonnell Genome Institute (MGI) using 10x Genomics GEM-X v3.4 chemistry.

CD45$^+$ single cells

For CD45$^+$ scRNA-seq, sciatic nerves from 5 to 9 mice were pooled per genotype for one replicate. The samples were processed using the same procedure described above until the myelin removal step. After myelin removal, cells were incubated in CD45$^+$ antibody (Invitrogen MCD4528; 1:250) for 20 min and FAC sorted using highly modified Beckman Coulter MoFlo at the Siteman Flow Cytometry core at Siteman Cancer Center. Additional debris and dead cells from the single cell suspensions were excluded during FAC sorting using propidium iodide (PI) as well. Cells were collected into PBS with 10% FBS prior to library preparation. The purified single cells were used to prepare scRNA-seq libraries following the 10X Genomics manufacturer's manuals at the GTAC @ MGI using 10X Genomics v3.1 chemistry.

Single cell/nucleus RNA-sequencing and analysis

All libraries were sequenced using Illumina NovaSeq 6000/X accordingly to the manufacturer's manuals at the GTAC @ MGI at Washington University in St. Louis. The reads were aligned to mouse genome version GRCm38/mm10 using CellRanger 8.0.1–7.1.0 from 10X Genomics which includes intronic reads in alignment by default. For nuclei, CellBender was used for ambient RNA removal (v0.3.0) [103], followed by QC filtering to remove nuclei with numbers of genes outside the threshold (nFeatures < 500 and > 7500) and high mitochondrial percentage (> 1%). Doublets were removed using Scrublet (v0.2.3) [104]. For single cell, the low-quality cells were removed from down-stream analysis by filtering for number of genes over the threshold (nFeatures < 500 and > 7500) and high mitochondrial percentage (> 10%). The single cell and single nuclei libraries were normalized by SCTransform (v2) and integrated using Harmony in Seurat (v5.1.0) in R (v2023.03.0) [105]. The CD45$^+$ libraries were normalized using SCTransform (v2) and integrated using the IntegrateData function in Seurat (v4.3.0) in R (v2023.03.0) [106]. The dimensions were reduced using principal component analysis (PCA) and visualized using UMAP. Standard Seurat pipeline was applied throughout the analysis process.

Cell type proportions test

T statistics of significant differences in the cell type proportions between groups were performed using the propeller method within the speckle R package (v1.4.0) [107]. The t-tests were moderated using an empirical Bayes framework.

Pseudo-bulk differentially expressed genes

Pseudo-bulk analysis was completed using DESeq2 (v1.44.0) which identifies differentially expressed genes between two groups of cells using a negative binomial distribution [108]. Each gene expression was aggregated by cluster and genotype. A standard DESeq pipeline was used to analyze differentially expressed genes and adjusted *p*-values. Volcano plots were generated using the EnhancedVolcano R package (v1.22.0) [109]. Visualized volcano plots include a $\log_2$FC cut-off of >|1| and an adjusted *p*-value cut-off of 0.05.

GO analysis

Gene Ontology (GO) terms associated with upregulated genes from the differential expression analysis were determined using clusterProfiler (v4.12.6) [110]. Standard clusterProfiler pipeline and visualization tools were used to assess and visualize.

Bulk RNA-sequencing analysis

Bulk RNA-sequencing was re-analyzed from previous literature as described [2]. These data were deposited in the Gene Expression Omnibus repository: ID GSE210403.

Spatial immunoassay via Akoya PhenoCycler

Flash frozen nerves from 2-3-month-old WT and *Nmnat2*$^{V98M/R232Q}$ mice were used for spatial immunoassay using Akoya Biosciences PhenoCycler-Fusion™ system (formerly known as CODEX). Mice were perfused with ice cold PBS. Nerves were collected, dried, embedded in OCT compound (PANTek Technologies 23-730-571), and flash frozen using dry ice. 6 µm-thick sections were prepared on a Leica CM1860 cryostat and mounted onto positively charged adhesive PERMASLIDE Plus (Leica 3800455). The prepared slides were store at -80˚C after sectioning prior to immunoassay. Immunoassay was performed at the Immunomonitoring (IML) Lab at the Bursky Center for Human Immunology & Immunotherapy Programs (CHiiPs) at Washington University in St. Louis. The following antibodies compatible with Akoya

PhenoCycler were examined: TUBB3, CD90.2 (30-H12), CD31 (MEC13.3), TCRb (H57-597), CD44 (IM7), Granzyme B, CD45 (30-F11), CD45R/B220 (Ra3-6B2), MHC II (M5/114.15.2), CD169 (3D6.112), IgD (11-26c.2a), NKP46/NCR1, CD19 (6D5), CD3 (17A2), CD24 (M1/69), CD21/35 (7E9), FoxP3 (MF-14), CD11b (M1/70), CD4 (RM4-5), PDL1 (10 F.9G2), CD8a (53 – 6.7), CD11c (N418), CX3CR1 (SA011F11), ICOS (C398.4 A), PDCA-1 (927), iNOS (W16030C), Ly6C (HK1.4), CD40 (3/23), Ki67 (B56), GL7, F4/80 (BM8). PhenoCycler images were analyzed using QuPath (v0.4.3) [111].

Multiplex cytokine/chemokine assay

A multiplex cytokine assay was used to simultaneously measure levels of multiple cytokines and chemokines in a single sample. Flash frozen sciatic nerves from 2-3-month-old WT, *Nmnat2*$^{V98M/R232Q}$, and nerve crushed WT mice at 1-, 3-, 5-, and 7-day post injury were analyzed using a customized Mouse Luminex Discovery Assay™ (R&D Systems LXSAMSM). Mice were euthanized and perfused with ice cold PBS. After the nerves were collected, the epineurium layers were removed in ice cold PBS with dry ice before flash freezing the nerves in liquid nitrogen. The samples were kept in -80˚C until further processing. Samples were pulverized using clean plastic blue pestles dipped in liquid nitrogen on dry ice and lysed using Procartaplex lysis buffer (Thermo Fisher EPX-99999-000) for 30 min on ice. A probe sonicator (Branson Digital Sonifier SFX 150) was used to sonicate the samples for 3 s at 40% amplitude. After sonication, samples were centrifuged at 14,000 g for 15 min at 4˚C to obtain supernatant. Total protein levels of each sample were obtained from a small aliquot and used to normalize all cytokine concentrations. The protein levels were measured on Luminex 200™ by the Immunomonitoring (IML) Lab at the Bursky Center for Human Immunology & Immunotherapy Programs (CHiiPs) at Washington University in St. Louis. The following cytokines were examined: Periostin, Chil3l, ICAM-1, uPAR, CCL8, IGF-1, CCL2, P-Selectin, CXCL16, IL-6, CXCL1, IL-4, VEGF, CCL22, IFNg, GM-CSF, and TNFa.

RNA fluorescence in situ hybridization

Sciatic nerves from 2-3-month-old WT and *Nmnat2*$^{V98M/R232Q}$ were harvested and fixed in 4% PFA for 1 h at room temperature and kept in 30% sucrose overnight at 4˚C. Nerve samples were dried and embedded in OCT compound, then frozen on dry ice and kept at -80˚C. 6 µm-thick sections were prepared on a Leica CM1860 cryostat, mounted onto positively charged slides, and stored at -80˚C. An ACDBio RNAscope™ Multiplex Fluorescent Reagent Kit v2 with the following RNA FISH probes was used: Mm-C3 (ACDBio 417841), Mm-Pdgfra-C2 (ACDBio 480661-C2), Mm-Cxcl14-C3 (ACDBio 459741-C3), Mm-Sox10-C4 (ACDBio 435931-C4). All steps were performed according to the manufacturer's manuals with a minor reduction in sample incubation time for Protease III application from 30 min to 15 min. A Leica Thunder Imaging System was used for fluorescent imaging at 20X and 40X magnification.

In situ images (20X section per mouse) were analyzed using ImageJ (v2.14.0/1.54f). Endoneurial cell masks were generated by thresholding the *Pdgfra* fluorescence channel, while Schwann cell masks were created by thresholding the *Sox10* fluorescence channel. Positive cells were identified using the 'Analyze Particles' function. Fluorescence intensity for *C3* and *Cxc14* was measured within Pdgfra$^+$ cells or Sox10$^+$ cells, respectively, and a threshold was selected to define positive cells. The percentage of positive cells within each corresponding mask was then calculated.

Tissue immunohistochemistry (IHC) staining

Sciatic nerves were harvested and fixed in 4% PFA for 1 h at room temperature and kept in 30% sucrose overnight at 4˚C. Nerve samples were dried and embedded in OCT compound, then frozen on dry ice. 6 µm-thick sections were prepared on a Leica CM1860 cryostat, mounted onto positively charged slides, and stored at -20˚C. The slides were washed in acetone for 10 min at -20˚C and dried completely. The slides were washed in PBS twice, then in PBS + 0.03% Triton™ X-100 (PBS-T) for 5 min. Slides were put into a staining tray with 10% normal goat serum (NGS) in PBS-T for an hour at RT. Slides were then incubated with primary antibodies diluted in 10% NGS and covered with parafilm in a 4˚C cold room overnight. The next day, slides were washed 3 times with PBS-T for 5 min at room temperature. Secondary antibodies were also diluted in 10% NGS and applied for an hour incubation. Slides were washed twice in PBS-T for 5 min at RT and once in PBS for the same duration. VECTASHIELD Hardset Antifade Mounting Medium with DAPI (Vector H-1500-10) was applied to the slides after drying the slides and a coverslip was put on. Final slides were stored in 4˚C. A Leica Thunder Imaging System was used to capture fluorescent images. The following primary antibodies were used: primary antibody Iba1 (1:500, Wako Chemicals, 019-19741), CD68 (1:100, Bio-Rad, MCA1957), and C1q (1:500, Abcam, Ab182451) and secondary antibody anti-rat Cy3 (1:500, Jackson Immunoresearch, 112-165-143) and anti-rabbit Alexa Fluor 488 (1:500, Invitrogen, A11034).

For C1q-stained samples, ImageJ (v2.14.0/1.54f) was used to quantify signal intensity from unprocessed whole-nerve images using 'Mean Gray Value' measurement function, with values normalized to the total nerve area. For Iba1- and CD68-stained samples, DAPI$^+$ cells displaying positive fluorescence for Iba1 and CD68 were

manually quantified using ImageJ. Quantification was performed on three nerve sections (20X) per mouse, with values normalized to the analyzed nerve area.

Flow cytometry

For flow cytometry analysis, mice were euthanized and perfused with PBS. Sciatic nerves were collected and kept on ice in DMEM with 1% FBS. Nerves were minced and incubated in the previously described digestion buffer at 37˚C for 30 min with gentle shaking. The samples were filtered through pre-wet 70-µm cell strainers and washed twice with DMEM with 1% FBS. Then myelin was removed using myelin removal beads II and LS columns following the Miltenyi Biotec protocol for myelin removal, as described above. Then the single cell suspensions were incubated with Zombie NIR fixable viability dye (BioLegend 423105) for 20 min in the dark and washed. Cells were resuspended in sorting buffer with CD16/32 FC block at a final concentration of 10 µg/mL (BioLegend 101301) for 5 min on ice in the dark and washed. Cells were incubated with fluorescently conjugated antibodies with Brilliant Stain Buffer Plus (BD Biosciences 566385) for 20 min at 4˚C in the dark and washed. Supernatant was decanted and cells were resuspended in fresh sorting buffer. Flow cytometry was performed on a Cytek Aurora Spectral CS at the Siteman Flow Cytometry core at the Siteman Cancer Center. The flow cytometry results were analyzed using BD Biosciences FlowJo (v10.10.0) software [112]. The following antibodies were used: CD4 (BD Biosciences 740208), CD11c (BD Biosciences 749039), TCRb (BD Biosciences 748405), CD19 (BD Biosciences 566107), IA/IE (BioLegend 107635), CD45 (BD Biosciences 746947), Ly6C (BioLegend 128022), CD8a (eBioscience 58-0081-80), CD64 (BioLegend 139304), CD117 (BioLegend 135108), F4/80 (BioLegend 123130). For IL1b (Invitrogen 12-7114-82) intracellular staining, a similar protocol was used with an addition of inhibitor cocktail adapted from Lasse Dissing-Olesen et al. [113] during enzymatic dissociation. Cells were washed and fixed in 4% PFA, and staining was completed using the BD Cytofix/Cytoperm kit (BD Biosciences 554714) per the manufacturer's manuals.

T cell depletion

Injection

Starting at two months of age, *Nmnat2*$^{V98M/R232Q}$ mice by intraperitoneally injected with 500 µg anti-mouse CD4 neutralizing antibody (InVivoPlus Bio X Cell BP0003-1) and 500 µg anti-mouse CD8a neutralizing antibody (InVivoPlus Bio X Cell BP0061) concurrently, or with 500 µg rat IgG2b (InVivoPlus Bio X Cell BP0090) once a week for three months. The inverted screen assay was administered prior to the first injection to measure the baseline motor function of each mouse at two months of age.

Inverted screen assay

The inverted screen assay was performed monthly according to the previously described method with minor modifications [2]. Mice were placed on a wire mesh screen, and after inverting the screen, the latency time to fall was recorded. Each mouse was assayed 4 times with a 5-minute rest in-between. The latency was averaged for each mouse after removing the lowest assay time to account for outliers. If a mouse did not fall off the screen within 120 s, then 120 s was recorded.

Axon area analysis

Femoral nerves were processed as previously described [2]. For light microscope analysis, sections were cut using a Leica EM UC7 Ultramicrotome and placed onto microscopy slides. Slides were then stained with 1% toluidine blue solution (1% toluidine blue, 2% borax), and washed with water, acetone, and xylene, and then mounted in Cytoseal XTL (Thermo Fisher Scientific 22-050-262) as previously described [2]. Whole nerves were imaged at 40X magnification using a Leica Thunder Imaging System, and 3 random fields were obtained using a 100X oil-immersion lens using a Nikon Eclipse 80i microscope. Axonal nerve area was measured and calculated based on 3 random fields of 100X images using MyelTracer (v1.3) [114].

Statistical analysis / illustrations

All statistics outside of the single cell analyses were performed using GraphPad Prism (v10.2.1). All illustrations created with BioRender.com.

Supplementary Information

The online version contains supplementary material available at https://doi.org/10.1186/s12974-025-03459-7.

Supplementary Material 1

Supplementary Material 2

Supplementary Material 3

Acknowledgements

We thank Milbrandt and DiAntonio lab members for technical support and insightful comments during this study, especially Cassidy Menendez. Special thanks to McDonnell Genome Institute Genome Technology Access Center for RNA-seq library preparation and sequencing, the Bursky Immunomonitoring Center for Luminex and multiplexing imaging support, and Flow Cytometry core at Siteman Cancer Center.

Author contributions

JC, YS, AD, JM conceived the overall study. All authors contributed to the study design. JC, AS performed the experiments and JC analyzed the data. HQL performed and analyzed additional flow cytometry and immunohistochemistry experiments. WD performed single nucleus QC and LB performed in situ staining. JC prepared the manuscript and figures. AJB, YS, SCJ, AD, JM oversaw the analysis and edited the manuscript. All authors gave final approval of the manuscript.

Funding
This work was supported by National Human Genome Research Institute T32 HG000045 grant to JC, National Institutes of Health grants NS133348 and NS087632 to AD and JM, the Needleman Center for Neurometabolism and Axonal Therapeutics, and the Bob and Signa Hermann Fund for Neuropathy Research.

Data availability
The datasets supporting the conclusions of this article are available in the Gene Expression Omnibus repository ID GSE291435 (WT and *Nmnat2* $^{V98M/R232Q}$ sc/snRNA-seq and CD45^{+} scRNA-seq) and GSE295346 (Sarm1-KO *Nmnat2* $^{V98M/R232Q}$ bulk RNA-seq). Previously published WT and *Nmnat2* $^{V98M/R232Q}$ sciatic bulk RNA-seq data were deposited in the Gene Expression Omnibus repository ID GSE210403. The source code for data analysis will be available online at https://github.com/cchoi217/Single-cell_Nmnat2.

Declarations

Competing interests
JM and AD are co-founders, scientific advisory board members, and shareholders of Disarm Therapeutics, a wholly owned subsidiary of Eli Lilly and scientific advisory board members of Asha Therapeutics. The authors have no other competing conflicts or financial interests.

Received: 24 February 2025 / Accepted: 1 May 2025
Published online: 23 May 2025

References

1. Coleman MP, Höke A. Programmed axon degeneration: from mouse to mechanism to medicine. Nat Rev Neurosci. 2020;21:183–96.
2. Dingwall CB, Strickland A, Yum SW, Yim AK, Zhu J, Wang PL, et al. Macrophage depletion blocks congenital SARM1-dependent neuropathy. J Clin Invest. 2022;132:e159800.
3. Figley MD, DiAntonio A. The SARM1 axon degeneration pathway: control of the NAD + metabolome regulates axon survival in health and disease. Curr Opin Neurobiol. 2020;63:59–66.
4. Krauss R, Bosanac T, Devraj R, Engber T, Hughes RO. Axons matter: the promise of treating neurodegenerative disorders by targeting SARM1-Mediated axonal degeneration. Trends Pharmacol Sci. 2020;41:281–93.
5. Gerdts J, Summers DW, Sasaki Y, DiAntonio A, Milbrandt J. Sarm1-mediated axon degeneration requires both SAM and TIR interactions. J Neurosci. 2013;33:13569–80.
6. Osterloh JM, Yang J, Rooney TM, Fox AN, Adalbert R, Powell EH, et al. dSarm/Sarm1 is required for activation of an injury-induced axon death pathway. Science. 2012;337:481–4.
7. Gilley J, Coleman MP. Endogenous Nmnat2 is an essential survival factor for maintenance of healthy axons. PLoS Biol. 2010;8:e1000300.
8. Yan T, Feng Y, Zheng J, Ge X, Zhang Y, Wu D, et al. Nmnat2 delays axon degeneration in superior cervical ganglia dependent on its NAD synthesis activity. Neurochem Int. 2010;56:101–6.
9. Figley MD, Gu W, Nanson JD, Shi Y, Sasaki Y, Cunnea K, et al. SARM1 is a metabolic sensor activated by an increased NMN/NAD + ratio to trigger axon degeneration. Neuron. 2021;109:1118–e113611.
10. Jiang Y, Liu T, Lee C-H, Chang Q, Yang J, Zhang Z. The NAD+-mediated self-inhibition mechanism of pro-neurodegenerative SARM1. Nature. 2020;588:658–63.
11. Essuman K, Summers DW, Sasaki Y, Mao X, DiAntonio A, Milbrandt J. The SARM1 Toll/Interleukin-1 receptor domain possesses intrinsic NAD + Cleavage activity that promotes pathological axonal degeneration. Neuron. 2017;93:1334–e13435.
12. Gerdts J, Brace EJ, Sasaki Y, DiAntonio A, Milbrandt J. SARM1 activation triggers axon degeneration locally via NAD^{+} destruction. Science. 2015;348:453–7.
13. Geisler S, Doan RA, Strickland A, Huang X, Milbrandt J, DiAntonio A. Prevention of vincristine-induced peripheral neuropathy by genetic deletion of SARM1 in mice. Brain. 2016;139:3092–108.
14. Sato-Yamada Y, Strickland A, Sasaki Y, Bloom J, DiAntonio A, Milbrandt J. A SARM1-mitochondrial feedback loop drives neuropathogenesis in a Charcot-Marie-Tooth disease type 2A rat model. J Clin Invest. 2022;132:e161566.
15. Turkiew E, Falconer D, Reed N, Höke A. Deletion of Sarm1 gene is neuroprotective in two models of peripheral neuropathy. J Peripheral Nerv Syst. 2017;22:162–71.
16. DiSabato DJ, Quan N, Godbout JP. Neuroinflammation: the devil is in the details. J Neurochem. 2016;139(Suppl 2):136–53.
17. Mammana S, Fagone P, Cavalli E, Basile MS, Petralia MC, Nicoletti F, et al. The role of macrophages in neuroinflammatory and neurodegenerative pathways of Alzheimer's disease, amyotrophic lateral sclerosis, and multiple sclerosis: pathogenetic cellular effectors and potential therapeutic targets. Int J Mol Sci. 2018;19:831.
18. Leng F, Edison P. Neuroinflammation and microglial activation in alzheimer disease: where do we go from here? Nat Rev Neurol. 2021;17:157–72.
19. Wang S, Sudan R, Peng V, Zhou Y, Du S, Yuede CM, et al. TREM2 drives microglia response to amyloid-β via SYK-dependent and -independent pathways. Cell. 2022;185:4153–e416919.
20. Liao B, Zhao W, Beers DR, Henkel JS, Appel SH. Transformation from a neuroprotective to a neurotoxic microglial phenotype in a mouse model of ALS. Exp Neurol. 2012;237:147–52.
21. Zigmond RE, Echevarria FD. Macrophage biology in the peripheral nervous system after injury. Prog Neurobiol. 2019;173:102–21.
22. Yuan X, Klein D, Kerscher S, West BL, Weis J, Katona I, et al. Macrophage depletion ameliorates peripheral neuropathy in aging mice. J Neurosci. 2018;38:4610–20.
23. Zhang H, Li Y, de Carvalho-Barbosa M, Kavelaars A, Heijnen CJ, Albrecht PJ, et al. Dorsal root ganglion infiltration by macrophages contributes to Paclitaxel Chemotherapy-Induced peripheral neuropathy. J Pain. 2016;17:775–86.
24. Starobova H, Mueller A, Deuis JR, Carter DA, Vetter I. Inflammatory and neuropathic gene expression signatures of Chemotherapy-Induced neuropathy induced by vincristine, cisplatin, and oxaliplatin in C57BL/6J mice. J Pain. 2020;21:182–94.
25. Keren-Shaul H, Spinrad A, Weiner A, Matcovitch-Natan O, Dvir-Szternfeld R, Ulland TK, et al. A unique microglia type associated with restricting development of Alzheimer's disease. Cell. 2017;169:1276–e129017.
26. Wang PL, Yim AKY, Kim K-W, Avey D, Czepielewski RS, Colonna M, et al. Peripheral nerve resident macrophages share tissue-specific programming and features of activated microglia. Nat Commun. 2020;11:2552.
27. Yim AKY, Wang PL, Bermingham JR, Hackett A, Strickland A, Miller TM, et al. Disentangling glial diversity in peripheral nerves at single-nuclei resolution. Nat Neurosci. 2022;25:238–51.
28. Lovatt D, Tamburino A, Krasowska-Zoladek A, Sanoja R, Li L, Peterson V, et al. scRNA-seq generates a molecular map of emerging cell subtypes after sciatic nerve injury in rats. Commun Biol. 2022;5:1–17.
29. Chen B, Banton MC, Singh L, Parkinson DB, Dun X. Single cell transcriptome data analysis defines the heterogeneity of peripheral nerve cells in homeostasis and regeneration. Front Cell Neurosci. 2021;15:624826.
30. Zhao X-F, Huffman LD, Hafner H, Athaiya M, Finneran MC, Kalinski AL et al. The injured sciatic nerve atlas (iSNAT), insights into the cellular and molecular basis of neural tissue degeneration and regeneration. Stevens B, Rothlin CV, Simons M, Carter BD, editors. eLife. 2022;11:e80881.
31. Gaedcke S, Sinning J, Dittrich-Breiholz O, Haller H, Soerensen-Zender I, Liao CM, et al. Single cell versus single nucleus: transcriptome differences in the murine kidney after ischemia-reperfusion injury. Am J Physiology-Renal Physiol. 2022;323:F171–81.
32. Bakken TE, Hodge RD, Miller JA, Yao Z, Nguyen TN, Aevermann B, et al. Single-nucleus and single-cell transcriptomes compared in matched cortical cell types. PLoS ONE. 2018;13:e0209648.
33. Arthur-Farraj PJ, Latouche M, Wilton DK, Quintes S, Chabrol E, Banerjee A, et al. c-Jun reprograms Schwann cells of injured nerves to generate a repair cell essential for regeneration. Neuron. 2012;75:633–47.
34. Lin G, Zhang H, Sun F, Lu Z, Reed-Maldonado A, Lee Y-C, et al. Brain-derived neurotrophic factor promotes nerve regeneration by activating the JAK/STAT pathway in Schwann cells. Translational Androl Urol. 2016;5:16775–16175.
35. Hu R, Dun X, Singh L, Banton MC. Runx2 regulates peripheral nerve regeneration to promote Schwann cell migration and re-myelination. Neural Regeneration Res. 2023;19:1575.
36. Bhatheja K, Field J. Schwann cells: origins and role in axonal maintenance and regeneration. Int J Biochem Cell Biol. 2006;38:1995–9.
37. Toma JS, Karamboulas K, Carr MJ, Kolaj A, Yuzwa SA, Mahmud N et al. Peripheral Nerve Single-Cell Analysis Identifies Mesenchymal Ligands that Promote Axonal Growth. eNeuro. 2020 [cited 2025 Apr 1];7. Available from: https://www.eneuro.org/content/7/3/ENEURO.0066-20.2020.

38. Cavagnero KJ, Gallo RL. Essential immune functions of fibroblasts in innate host defense. Front Immunol. 2022 [cited 2025 Feb 12];13. Available from: https://www.frontiersin.org/journals/immunology/articles/10.3389/fimmu.2022.1058862/full
39. Davidson S, Coles M, Thomas T, Kollias G, Ludewig B, Turley S, et al. Fibroblasts as immune regulators in infection, inflammation and cancer. Nat Rev Immunol. 2021;21:704–17.
40. Kendall RT, Feghali-Bostwick CA. Fibroblasts in fibrosis: novel roles and mediators. Front Pharmacol. 2014;5:123.
41. Lee B, Lee S-H, Shin K. Crosstalk between fibroblasts and T cells in immune networks. Front Immunol. 2023 [cited 2025 Feb 12];13. Available from: https://www.frontiersin.org/journals/immunology/articles/10.3389/fimmu.2022.1103823/full
42. Köhler J, Maletzki C, Koczan D, Frank M, Springer A, Steffen C, et al. Kininogen supports inflammation and bacterial spreading during Streptococccus pyogenes Sepsis. EBioMedicine. 2020;58:102908.
43. Zhao X, Sato A, Dela Cruz CS, Linehan M, Luegering A, Kucharzik T, et al. CCL9 is secreted by the Follicle-Associated epithelium and recruits dome region Peyer's patch CD11b + Dendritic cells 1. J Immunol. 2003;171:2797–803.
44. Li B, Li W, Liang Y, Zhang C, Kong G, Li Z. Spleen-Derived CCL9 recruits MDSC to facilitate tumor growth in orthotopic hepatoma mice. Glob Med Genet. 2023;10:348–56.
45. Disteldorf EM, Krebs CF, Paust H-J, Turner J-E, Nouailles G, Tittel A, et al. CXCL5 drives neutrophil recruitment in TH17-Mediated GN. J Am Soc Nephrology: JASN. 2014;26:55.
46. Leemans JC, te Velde AA, Florquin S, Bennink RJ, de Bruin K, van Lier RAW, et al. The epidermal growth Factor-Seven transmembrane (EGF-TM7) receptor CD97 is required for neutrophil migration and host Defense1. J Immunol. 2004;172:1125–31.
47. Su Q, Li L, Li X, Li W, Zhang X, Dong Y, et al. CD97 serves as a novel biomarker of immune cell infiltration in hepatocellular carcinoma. World J Surg Oncol. 2022;20:382.
48. Safaee MM, Wang EJ, Jain S, Chen J-S, Gill S, Zheng AC, et al. CD97 is associated with mitogenic pathway activation, metabolic reprogramming, and immune microenvironment changes in glioblastoma. Sci Rep. 2022;12:1464.
49. Dadwal N, Mix C, Reinhold A, Witte A, Freund C, Schraven B, et al. The multiple roles of the cytosolic adapter proteins ADAP, SKAP1 and SKAP2 for TCR/CD3 -Mediated signaling events. Front Immunol. 2021;12:703534.
50. Cohen MC, Cohen S. Cytokine function: a study in biologic diversity. Am J Clin Pathol. 1996;105:589–98.
51. Zhang J-M, An J. Cytokines, inflammation and pain. Int Anesthesiol Clin. 2007;45:27–37.
52. Kumar A, Mohamed E, Tong S, Chen K, Mukherjee J, Lim Y, et al. CXCL14 promotes a robust brain Tumor-Associated immune response in glioma. Clin Cancer Res. 2022;28:2898–910.
53. Lu J, Chatterjee M, Schmid H, Beck S, Gawaz M. CXCL14 as an emerging immune and inflammatory modulator. J Inflamm. 2016;13:1.
54. DaMata JP, Zelkoski AE, Nhan PB, Ennis KHE, Kim JS, Lu Z, et al. Dissociation protocols influence the phenotypes of lymphocyte and myeloid cell populations isolated from the neonatal lymph node. Front Immunol. 2024;15:1368118.
55. Wu T, Dejanovic B, Gandham VD, Gogineni A, Edmonds R, Schauer S, et al. Complement C3 is activated in human AD brain and is required for neurodegeneration in mouse models of amyloidosis and tauopathy. Cell Rep. 2019;28:2111–e21236.
56. Lee JD, Levin SC, Willis EF, Li R, Woodruff TM, Noakes PG. Complement components are upregulated and correlate with disease progression in the TDP-43Q331K mouse model of amyotrophic lateral sclerosis. J Neuroinflamm. 2018;15:171.
57. Bahia El Idrissi N, Bosch S, Ramaglia V, Aronica E, Baas F, Troost D. Complement activation at the motor end-plates in amyotrophic lateral sclerosis. J Neuroinflamm. 2016;13:72.
58. Watkins LM, Neal JW, Loveless S, Michailidou I, Ramaglia V, Rees MI, et al. Complement is activated in progressive multiple sclerosis cortical grey matter lesions. J Neuroinflamm. 2016;13:161.
59. Engel AG, Lambert EH, Howard FM. Immune complexes (IgG and C3) at the motor end-plate in myasthenia Gravis: ultrastructural and light microscopic localization and electrophysiologic correlations. Mayo Clin Proc. 1977;52:267–80.
60. Lennon VA, Seybold ME, Lindstrom JM, Cochrane C, Ulevitch R. Role of complement in the pathogenesis of experimental autoimmune myasthenia Gravis. J Exp Med. 1978;147:973–83.
61. Li M, Peake PW, Charlesworth JA, Tracey DJ, Moalem-Taylor G. Complement activation contributes to leukocyte recruitment and neuropathic pain following peripheral nerve injury in rats. Eur J Neurosci. 2007;26:3486–500.
62. Xu J, Zhang L, Xie M, Li Y, Huang P, Saunders TL, et al. Role of complement in a rat model of Paclitaxel-Induced peripheral neuropathy. J Immunol. 2018;200:4094–101.
63. Dunkelberger JR, Song W-C. Complement and its role in innate and adaptive immune responses. Cell Res. 2010;20:34–50.
64. Hsu MH, Ember JA, Wang M, Prossnitz ER, Hugli TE, Ye RD. Cloning and functional characterization of the mouse C3a anaphylatoxin receptor gene. Immunogenetics. 1997;47:64–72.
65. Kaul M, Loos M. Collagen-like complement component C1q is a membrane protein of human monocyte-derived macrophages that mediates endocytosis. J Immunol. 1995;155:5795–802.
66. Wolbert J, Li X, Heming M, Mausberg AK, Akkermann D, Frydrychowicz C, et al. Redefining the heterogeneity of peripheral nerve cells in health and autoimmunity. Proc Natl Acad Sci U S A. 2020;117:9466–76.
67. Silvin A, Uderhardt S, Piot C, Da Mesquita S, Yang K, Geirsdottir L, et al. Dual ontogeny of disease-associated microglia and disease inflammatory macrophages in aging and neurodegeneration. Immunity. 2022;55:1448–e14656.
68. Brennan FH, Li Y, Wang C, Ma A, Guo Q, Li Y, et al. Microglia coordinate cellular interactions during spinal cord repair in mice. Nat Commun. 2022;13:4096.
69. Caronni N, La Terza F, Vittoria FM, Barbiera G, Mezzanzanica L, Cuzzola V, et al. IL-1β + macrophages fuel pathogenic inflammation in pancreatic cancer. Nature. 2023;623:415–22.
70. Zhou Z, Zhou X, Jiang X, Yang B, Lu X, Fei Y, et al. Single-cell profiling identifies IL1Bhi macrophages associated with inflammation in PD-1 inhibitor-induced inflammatory arthritis. Nat Commun. 2024;15:2107.
71. Chen X, Firulyova M, Manis M, Herz J, Smirnov I, Aladyeva E, et al. Microglia-mediated T cell infiltration drives neurodegeneration in tauopathy. Nature. 2023;615:668–77.
72. Clarkson BDS, Grund EM, Standiford MM, Mirchia K, Westphal MS, Muschler LS et al. $CD8^+$ T cells recognizing a neuron-restricted antigen injure axons in a model of multiple sclerosis. J Clin Invest. 2023 [cited 2025 Jan 14];133. Available from: https://www.jci.org/articles/view/162788
73. Subbarayan MS, Hudson C, Moss LD, Nash KR, Bickford PC. T cell infiltration and upregulation of MHCII in microglia leads to accelerated neuronal loss in an α-synuclein rat model of Parkinson's disease. J Neuroinflammation. 2020;17:242.
74. Gate D, Tapp E, Leventhal O, Shahid M, Nonninger TJ, Yang AC, et al. CD4 + T cells contribute to neurodegeneration in lewy body dementia. Science. 2021;374:868–74.
75. Garber C, Soung A, Vollmer LL, Kanmogne M, Last A, Brown J, et al. T cells promote microglia-mediated synaptic elimination and cognitive dysfunction during recovery from neuropathogenic flaviviruses. Nat Neurosci. 2019;22:1276–88.
76. Gate D, Saligrama N, Leventhal O, Yang AC, Unger MS, Middeldorp J, et al. Clonally expanded CD8 T cells patrol the cerebrospinal fluid in Alzheimer's disease. Nature. 2020;577:399–404.
77. Merlini M, Kirabali T, Kulic L, Nitsch RM, Ferretti MT. Extravascular CD3 + T cells in brains of alzheimer disease patients correlate with Tau but not with amyloid pathology: an immunohistochemical study. Neurodegener Dis. 2018;18:49–56.
78. Schneider-Hohendorf T, Schwab N, Uçeyler N, Göbel K, Sommer C, Wiendl H. CD8 + T-cell immunity in chronic inflammatory demyelinating polyradiculoneuropathy. Neurology. 2012;78:402–8.
79. Seyedsadr M, Bang MF, McCarthy EC, Zhang S, Chen H-C, Mohebbi M et al. A pathologically expanded, clonal lineage of IL-21–producing $CD4^+$ T cells drives inflammatory neuropathy. J Clin Invest. 2024 [cited 2025 Jan 13];134. Available from: https://www.jci.org/articles/view/178602
80. Súkeníková L, Mallone A, Schreiner B, Ripellino P, Nilsson J, Stoffel M, et al. Autoreactive T cells target peripheral nerves in Guillain–Barré syndrome. Nature. 2024;626:160–8.
81. Wang T, Lee M-H, Choi E, Pardo-Villamizar CA, Lee SB, Yang IH, et al. Granzyme B-Induced neurotoxicity is mediated via activation of PAR-1 receptor and Kv1.3 channel. PLoS ONE. 2012;7:e43950.
82. Roche PA, Furuta K. The Ins and outs of MHC class II-mediated antigen processing and presentation. Nat Rev Immunol. 2015;15:203–16.
83. Streit WJ, Mrak RE, Griffin WST. Microglia and neuroinflammation: a pathological perspective. J Neuroinflamm. 2004;1:14.

84. Adamu A, Li S, Gao F, Xue G. The role of neuroinflammation in neurodegenerative diseases: current Understanding and future therapeutic targets. Front Aging Neurosci. 2024;16:1347987.
85. Dingwall CB, Sasaki Y, Strickland A, Summers DW, Bloom AJ, DiAntonio A et al. Suppressing phagocyte activation by overexpressing the phosphatidylserine lipase ABHD12 preserves sarmopathic nerves. bioRxiv; 2024 [cited 2025 Apr 1]. p. 2024.06.20.599919. Available from: https://www.biorxiv.org/content/10.1101/2024.06.20.599919v1
86. Yang X, Lin Y, Shi Y, Li B, Liu W, Yin W, et al. FAP promotes immunosuppression by Cancer-Associated fibroblasts in the tumor microenvironment via STAT3–CCL2 signaling. Cancer Res. 2016;76:4124–35.
87. Xu H, Zhao J, Li J, Zhu Z, Cui Z, Liu R, et al. Cancer associated fibroblast–derived CCL5 promotes hepatocellular carcinoma metastasis through activating HIF1α/ZEB1 axis. Cell Death Dis. 2022;13:1–13.
88. Lee H-J, Suk J-E, Patrick C, Bae E-J, Cho J-H, Rho S, et al. Direct transfer of α-Synuclein from neuron to astroglia causes inflammatory responses in Synucleinopathies *. J Biol Chem. 2010;285:9262–72.
89. Païdassi H, Tacnet-Delorme P, Garlatti V, Darnault C, Ghebrehiwet B, Gaboriaud C, et al. C1q binds phosphatidylserine and likely acts as a Multiligand-Bridging molecule in apoptotic cell recognition. J Immunol. 2008;180:2329–38.
90. Hong S, Beja-Glasser VF, Nfonoyim BM, Frouin A, Li S, Ramakrishnan S, et al. Complement and microglia mediate early synapse loss in alzheimer mouse models. Science. 2016;352:712–6.
91. Groh J, Basu R, Stanley ER, Martini R. Cell-Surface and secreted isoforms of CSF-1 exert opposing roles in Macrophage-Mediated neural damage in Cx32-Deficient mice. J Neurosci. 2016;36:1890–901.
92. Starobova H, Monteleone M, Adolphe C, Batoon L, Sandrock CJ, Tay B, et al. Vincristine-induced peripheral neuropathy is driven by canonical NLRP3 activation and IL-1β release. J Exp Med. 2021;218:e20201452.
93. Elyaman W, Stern LJ, Jiang N, Dressman D, Bradley P, Klatzmann D et al. Exploring the role of T cells in Alzheimer's and other neurodegenerative diseases: Emerging therapeutic insights from the T Cells in the Brain symposium. Alzheimer's & Dementia. n/a:e14548.
94. Williams GP, Schonhoff AM, Jurkuvenaite A, Gallups NJ, Standaert DG, Harms AS. CD4 T cells mediate brain inflammation and neurodegeneration in a mouse model of Parkinson's disease. Brain. 2021;144:2047–59.
95. Zeng J, Liao Z, Yang H, Wang Q, Wu Z, Hua F, et al. T cell infiltration mediates neurodegeneration and cognitive decline in Alzheimer's disease. Neurobiol Dis. 2024;193:106461.
96. Klein D, Martini R. Myelin and macrophages in the PNS: an intimate relationship in trauma and disease. Brain Res. 2016;1641:130–8.
97. Ostertag C, Klein D, Martini R. Presymptomatic macrophage targeting has a long-lasting therapeutic effect on treatment termination in a mouse model of Charcot-Marie-Tooth 1. Exp Neurol. 2022;357:114195.
98. Mäurer M, Kobsar I, Berghoff M, Schmid CD, Carenini S, Martini R. Role of immune cells in animal models for inherited neuropathies: facts and visions. J Anat. 2002;200:405–14.
99. Haile Y, Simmen KC, Pasichnyk D, Touret N, Simmen T, Lu J-Q, et al. Granule-Derived granzyme B mediates the vulnerability of human neurons to T Cell-Induced neurotoxicity. J Immunol. 2011;187:4861–72.
100. Abdelwahab T, Stadler D, Knöpper K, Arampatzi P, Saliba A-E, Kastenmüller W, et al. Cytotoxic CNS-associated T cells drive axon degeneration by targeting perturbed oligodendrocytes in *PLP1* mutant mice. iScience. 2023;26:106698.
101. Martini R, Toyka KV. Immune-mediated components of hereditary demyelinating neuropathies: lessons from animal models and patients. Lancet Neurol. 2004;3:457–65.
102. Younger DS, Rosoklija G, Hays Ap, Trojaborg W, Latov N. Diabetic peripheral neuropathy: A clinicopathologic and immunohistochemical analysis of Sural nerve biopsies. Muscle Nerve. 1996;19:722–7.
103. Fleming SJ, Chaffin MD, Arduini A, Akkad A-D, Banks E, Marioni JC, et al. Unsupervised removal of systematic background noise from droplet-based single-cell experiments using cellbender. Nat Methods. 2023;20:1323–35.
104. Wolock SL, Lopez R, Klein AM, Scrublet. Computational identification of cell doublets in Single-Cell transcriptomic data. Cell Syst. 2019;8:281–e2919.
105. Korsunsky I, Millard N, Fan J, Slowikowski K, Zhang F, Wei K, et al. Fast, sensitive and accurate integration of single-cell data with harmony. Nat Methods. 2019;16:1289–96.
106. Satija R, Farrell JA, Gennert D, Schier AF, Regev A. Spatial reconstruction of single-cell gene expression data. Nat Biotechnol. 2015;33:495–502.
107. Phipson B, Sim CB, Porrello ER, Hewitt AW, Powell J, Oshlack A. Propeller: testing for differences in cell type proportions in single cell data. Bioinformatics. 2022;38:4720–6.
108. Love MI, Huber W, Anders S. Moderated Estimation of fold change and dispersion for RNA-seq data with DESeq2. Genome Biol. 2014;15:550.
109. Blinghe K, Rana S, Lewis M. EnhancedVolcano: publication-ready volcano plots with enhanced colouring and labeling. 2024. Available from: https://github.com/kevinblighe/EnhancedVolcano
110. Yu G, Wang L-G, Han Y, He Q-Y. ClusterProfiler: an R package for comparing biological themes among gene clusters. OMICS. 2012;16:284–7.
111. Bankhead P, Loughrey MB, Fernández JA, Dombrowski Y, McArt DG, Dunne PD, et al. QuPath: open source software for digital pathology image analysis. Sci Rep. 2017;7:16878.
112. Becton D, et al. FlowJo™ software. Ashland OR: Dickinson and Company; 2023.
113. Dissing-Olesen L, Walker AJ, Feng Q, Barr HJ, Walker AC, Xie L, et al. FEAST: A flow cytometry-based toolkit for interrogating microglial engulfment of synaptic and Myelin proteins. Nat Commun. 2023;14:6015.
114. Kaiser T, Allen HM, Kwon O, Barak B, Wang J, He Z et al. MyelTracer: A Semi-Automated software for Myelin g-Ratio quantification. eNeuro. 2021;8:ENEURO.0558-20.

Publisher's note